Mathematical modeling of endocrine regulation subject to circadian rhythm

Medvedev, Alexander; Proskurnikov, Anton V.; Zhusubaliyev, Zhanybai T.

DOI
10.1016/j.arcontrol.2018.08.002

Publication date
2018

Document Version
Accepted author manuscript

Published in
Annual Reviews in Control

Mathematical modeling of endocrine regulation subject to circadian rhythm

Alexander Medvedev[a,1,*], Anton V. Proskurnikov[b,c], Zhanybai T. Zhusubaliyev[d]

[a] *Department of Information Technology, Uppsala University, Lägerhyddsvägen 2, SE-751 05, Uppsala, Sweden.*
[b] *Delft Center for Systems and Control, Delft University of Technology, Mekelweg 2, 2628 CD, Delft, The Netherlands*
[c] *Institute for Problems of Mechanical Engineering of the Russian Academy of Sciences (IPME RAS), St. Petersburg, Russia*
[d] *Department of Computer Science, Southwest State University, 50 Years of October Str. 94, 305040, Kursk, Russia.*

Abstract

The 2017 Nobel Prize in Physiology or Medicine awarded for discoveries of molecular mechanisms controlling the circadian rhythm has called attention to the challenging area of nonlinear dynamics that deals with synchronization and entrainment of oscillations. Biological circadian clocks keep time in living organisms, orchestrating hormonal cycles and other periodic rhythms. The periodic oscillations of circadian pacemakers are self-sustained; at the same time, they are *entrainable* by external periodic signals that adjust characteristics of autonomous oscillations. Whereas modeling of biological oscillators is a well-established research topic, mathematical analysis of *entrainment*, i.e. the nonlinear phenomena imposed by periodic exogenous signals, remains an open problem. Along with sustained periodic rhythms, periodically forced oscillators can exhibit various "irregular" behaviors, such as quasiperiodic or chaotic trajectories.

In this paper, we present an overview of the mathematical models of circadian rhythm with respect to endocrine regulation, as well as biological background. Dynamics of the human endocrine system, comprising numerous glands and hormones operating under neural control, are highly complex. Therefore, only endocrine subsystems (or *axes*) supporting certain biological functions are usually studied. Low-order dynamical models that capture the essential characteristics and interactions between a few hormones can than be derived. Goodwin's oscillator often serves as such a model and widely regarded as a prototypical biological oscillator. A comparative analysis of forced dynamics arising in two versions of Goodwin's oscillator is provided in the present paper: the classical continuous oscillator and a more recent impulsive one, capturing e.g. pulsatile secretion of hormones due to neural regulation. The main finding of this study is that, while the continuous oscillator is always forced to a periodic solution by a sufficiently large exogenous signal amplitude, the impulsive one commonly exhibits a quasiperiodic or chaotic behavior due to non-smooth dynamics in entrainment.

Keywords: Biomedical systems, Nonlinear dynamics, Synchronization, Entrainment, Hybrid Systems, Impulse signals.

1. Introduction

On October 2, 2017, the Nobel Assembly at *Karolinska Institutet* has decided to award the 2017 Nobel Prize in Physiology or Medicine jointly to Jeffrey C. Hall, Michael Rosbash, and Michael W. Young for their discoveries of molecular mechanisms controlling the circadian rhythm, [1]. Throughout the whole history of the Nobel Prize since 1901, this is arguably the first time, when the awarded discoveries are so closely related to the areas of dynamical systems, nonlinear control, and synchronization.

The Nobel Assembly states further that "Their discoveries explain how plants, animals and humans adapt their biological rhythm so that it is synchronized with the Earth's revolutions." The Nobel Prize winners' main contributions (see e.g. [2–4]) and historical milestones in studying circadian clocks are surveyed in [5].

The purpose of this review is to look into mathematical models that capture the mechanism of biological synchronization and to demonstrate their capability to explain a diversity of phenomena due to circadian rhythm observed in the endocrine system of an organism.

In biological systems, particularly in endocrine regulation, the control laws are designed by nature and are, typically, highly nonlinear. Further, in pulsatile feedback regulation, widely implemented in numerous endocrine loops, the dynamics are as well non-smooth. Restricting consideration of the present paper to only analytical approaches would not cover a fraction of the possible non-linear behaviours. Therefore, bifurcation analysis becomes necessary in order to reveal and study the complexity of the dynamics arising in endocrine loops subject to periodic

*Corresponding author.
Email addresses: alexander.medvedev@it.uu.se (Alexander Medvedev), anton.p.1982@ieee.org (Anton V. Proskurnikov), zhanybai@hotmail.com (Zhanybai T. Zhusubaliyev)

[1] A. Medvedev was in part financed by Grant 2015-05256 from the Swedish Research Council. The work of A.V. Proskurnikov is supported by Russian Foundation for Basic Research grants 17-08-01728, 17-08-00715 and 17-08-01266. The work on Theorem 2 is supported solely by Russian Science Foundation grant 16-19-00057 held by IPME RAS.

exogenous signals, e.g. circadian rhythm.

1.1. Circadian clock and circadian rhythm

The life on Earth is greatly influenced by the rotation of the planet. Most of the organisms, from microbes to mammals [6], are able to anticipate the environmental changes following the day-night cycle and adapt to them. The arising 24 hours pattern is called *circadian rhythm*, to simply indicate that the period of it is approximately a day: the Latin words *circa* meaning "around" and *dies* meaning "day". Experimental investigations of circadian rhythms in biology date back to the 18th century , when the astronomer Jean Jacques d'Ortous de Mairan studied *Mimosa pudica* plants [7]. He noticed that the leaves of the plant were directed towards the sun during daytime and then closed at dusk. Even when the plants were isolated from sunlight , their leaves continued to follow their normal daily oscillation. The heliotrope flower thus does not respond to the Sun motion; its rhythm is controlled by some endogenous mechanism. De Mairan also conjectured the possibility to influence this mechanism (e.g. to reverse the order of day and night) by artificial lighting; such experiments were later conducted by de Candolle [8] who also discovered that the free-running period of *Mimosa pudica* rhythm was discernibly less than the solar day and varied between 22 and 23 hours. As a result of these experiments , a clear evidence of an internal clock controlling the plant behavior has emerged. The circadian clock is entrained by external cues, called *zeitgebers* ("time givers" in German) such as sunlight, food intake, physical activity, temperature variations, social rhythms, etc. A mechanism of adaptation to environmental change, entrainment is a fundamental notion in the circadian rhythm regulation. Entrainment is also referred to as forced synchronization [9], being a special kind of synchronization that occurs in dynamical systems under external forces.

1.2. Cell level of circadian clock

In 1970's, a gene responsible for the circadian rhythm has been discovered in experiments with *Drosophila* by Ronald Konopka working in the lab of Seymour Benzer at the California Institute of Technology, [10]. A mutation in this gene named *period* (*Per*) has led to disruption in the circadian rhythm of flies, manifesting itself in their late eclosion and altered patterns of locomotor activity. Along with earlier works on genetic regulation of protein synthesis [11], Konopka's discovery has become a breakthrough in understanding genetic control mechanisms.

The circadian clock within a cell is a series of biochemical reactions, involving so-called clock proteins, that gives rise to a sustained oscillation (a limit cycle) through a dynamical feedback mechanism. A negative feedback of gene expression is thus a necessary part of the molecular mechanism of circadian oscillations. These circadian rhythms can occur under constant environmental conditions and are therefore endogenous. At the same time, the circadian clock is *adjusted* to the environment via the entrainment of circadian rhythms by light-dark (LD) cycles. Most of the molecular studies of circadian rhythms were first performed on *Drosophila* and *Neurospora* but have been extended further to cyanobacteria, plants, and mammals [12–15]. Simplified circadian clock models used Hill-type terms [16] for transcription regulation and Michaelis-Menten type [17] or delay terms for posttranslation regulation. In the absence of external disturbances, the solutions of such models usually either converge to limit cycles or stable equilibria.

The extensive mathematical model in [14] portrays the mammal circadian clock by means of 16 differential equations. This model possesses periodic solutions within a wide biologically supported range of parameters. The free running period of the model, i.e. in absence of external cues, varies between 46.4 h and 14.3 h, when the model parameters are set to their maximal and minimal values, one by one. A detailed mathematical (stochastic) model of the circadian clock found in mouse cells is build in [15] and involves altogether 36 reactions. It exhibits a free running limit cycle of 24.299 h and can be entrained to 24 h day by interchanging periods of light and darkness, 12 h each.

The simulation models in [14, 15] exploit the full available knowledge about biochemical reactions regulating the mammal's circadian clock. When implemented, the models produce periodic solutions in continuous darkness (free run) with realistic temporal characteristics; this periodic solutions are entrainable by suitable LD cycles. The changes in the period and phase of the circadian rhythm under such entrainment naturally depend on the model's parameters. Pathological phase locking is observed in e.g. familial advanced sleep phase syndrome, a lifelong disorder characterized by a pattern of sleep onset around 7:30 p.m. and offset around 4:30 a.m. The condition has been shown to be related to genetic mutations [18] and has been reproduced in genetically modified animals [19].

An interesting insight obtained in [14] is that (periodical) entrainment to LD cycles occurs only in a limited parametric and state subspaces, while the rest of the solutions are quasi-periodic in nature. The latter means that the phase of the model solution does not lock to the phase of the LD cycle. The authors produce a biological explanation to this phenomenon related to the levels of the protein CRY in the cell, with other model variables potentially involved. Typically, a domain of entrainment to LD cycles is flanked by two areas where periodical solutions do not occur. Therefore, one can assert that entrainment is not a universal property of the circadian clock and depends on both the clock's performance and environmental signals. The same statement is presumably also true with respect to pulsatile endocrine systems.

1.3. Suprachiasmatic nucleus

Although each cell possesses a circadian clock, in mammals, there is a higher level pacemaker center in the hypothalamus, which is called the suprachiasmatic nucleus

(SCN) and sometimes termed as the "master clock" of the brain. The SCN serves as best example of a brain center with a single dedicated function. The individual neurons comprising the SCN can independently continue to keep time, when dispersed in culture. Within the SCN, all the neurons (approximately 20.000) are tightly synchronized. The circadian rhythm is collectively produced by the neurons of the SCN. A certain transcription factor, *Lhx1*, enables communication between the cells in the SCN [20]. In the absence of hypothalamic *Lhx1*, the cells of the SCN still maintain oscillation but, as a loosely connected group, are unable to develop a strong circadian pattern without a daily light signal synchronizing their activity. The circadian clocks in cells of other tissues of the organism synchronize to the rhythm of the SCN, thereby creating a hierarchical time-keeping structure. Actually, the SCN is the only mammalian oscillator entrained by light, through the *Lhx1* gene that is strongly suppressed by light. The light signals recieved by the hypothalamus from the retina are passed on by the SCN into the pineal gland that produces melatonin [21], the hormone regulating sleep and wakefulness. The full mechanism of SCN functioning is not fully understood; recent experiments have revealed a tight coupling between the genetically controlled mechanism of the SCN pacemaker and oscillations in metabolic oxidation-reduction (redox) reactions [22, 23]. Redox reactions modulate membrane excitability and ion channel gates of the SCN neurons, influencing neuronal activity [23].

The role of strong synchronization in the SCN is to robustify the circadian rhythm against phase shifts in the firing of individual neurons, neural noise, and other exogenous impacting factors. However, no mechanism for fast adjustment of the circadian rhythm has appeared during mammalian evolution. For this reason, long-haul air passengers suffer from jet lag [24]. Clinical symptoms of jet lag consist of insomnia, sleepiness, neural (fatigue, headaches, and irritability) and cognitive impairments (concentration, judgment and memory disturbance), [25]. Jet lag severity is individual but also clearly depends on the number of passed time zones, i.e. the magnitude of the phase shift. The highly nonlinear nature of entrainment gives rise to asymmetric phase response to time difference: eastward jet lag is worse than the westward kind. Note that this is consistent with the already mentioned observation of the free-running circadian rhythm being slightly less than 24 hours. The robustness of the circadian clock against disturbances leads to a long transient in response to a drastic change in the phase of the day-night cycle. In spite of a rapid phase shift within the SCN , it can take many days to reset circadian rhythm in other parts of the brain and the peripheral tissue [25].

1.4. Circadian rhythm in endocrine regulation

Specialization of cells in a multi-cellular organism is essentially possible due to the communication mechanisms, where some cells produce signals and other ones respond to them in a certain biological manner. In mammals, actions and interactions of two communication systems - nervous and endocrine - underlie every regulatory mechanism of the body. The former makes use of fast electrical signaling, while the latter utilizes slow chemical imparting means.

Hormones act as chemical messengers from one cell (or a group of cells) to another, and are produced by nearly every organ and tissue type in a multi-cellular organism. Hormones are secreted mainly in endocrine glands directly into the blood stream and can potentially signal all cells in an organism that are reached by the blood.

Endocrine regulation. Hormonal (endocrine) regulation is a complex dynamic biological system, where hormones, often represented as their serum concentrations, interact via numerous feedback and feedforward mechanisms [26, 27] that can be stimulatory (positive) or inhibitory (negative) and lead, respectively, to an increase or a decrease in the hormone's production. Hormone secretion can also be in one of two distinct modes, namely, continuous or pulsatile [28]. While continuously secreted hormones can be suitably captured in mathematical modelling as an inflow and described by a differential equation, pulsatile secretion demands a formalism of impulsive and hybrid systems theory in order to quantify the number, size, and shape of secretory bursts. Pulsatility is a physiological mechanism of rapid adjustment of hormone concentrations and communicating signaling information to target tissues. The loop of interacting hormones in an organism is closed and dynamically stable, which properties guarantee homeostasis, i.e. biological self-regulation. In endocrine loops with pulsatile secretion, homeostasis corresponds to sustained oscillations rather than staying at an equilibrium; already the seminal publication on homeostasis [29] actually recognizes oscillation as a possible form of homeostatic condition.

Circadian rhythm is known to influence the dynamical behavior of endocrine systems, by e.g. modulating the hormone levels [30]. While the SCN is central to the regulation of some hormones, such as melatonin, the local molecular clock implemented in endocrine tissue plays a critical role in regulation of e.g. insulin and cortisol [31]. Known also as the stress hormone, cortisol controls response to stress and anxiety, exhibiting one of the most distinct circadian rhythm in humans. In healthy individuals, levels of cortisol are very low or almost undetectable at midnight and then build up to peak in the morning (7:00–8:00) and prepare thus the organism to physical activity. It has been suggested [32] that cortisol acts as a secondary messenger between the SCN and peripheral clocks and is involved in synchronization of all bodily circadian rhythms.

Cortisol regulation. Secretion of cortisol by the adrenal cortex is controlled by adrenocorticotropin hormone (ACTH) produced by the anterior pituitary gland. ACTH release is in turn controlled by corticotropin-releasing hormone (CRH). Cortisol has negative feedback effect on both

the hypothalamus and the anterior pituitary, inhibits respectively the formation of CRH and the synthesis of ACTH. These mechanisms constitute a classical negative feedback loop, whose response time is within several minutes. Since the CRH secretion site and the SCN are located in the hypothalamus , the action of the SCN on the cortisol regulation involves neuronal connection with hypothalamic neurosecretory neurons [33]. Yet, there is no feedback on the SCN and thus the effect of the central circadian clock can be seen as an exogenous signal with respect to the closed loop of cortisol regulation. The adrenal gland contains a (local) circadian clock that is retarded six hours in phase with respect to the oscillation in the SCN [32].

Testosterone regulation. The pulsatile activity of the hypothalamus is also prominent in regulation of other hormones, for instance testosterone. In the endocrine system of testosterone (Te) regulation in the male, an essential role is played by the luteinizing hormone (LH) and gonadotropin-releasing hormone (GnRH). While Te is produced in Leydig cells of testes, LH and GnRH are secreted in different parts of the brain, i.e. in the hypophysis (pituitary gland) and the hypothalamus, respectively. The pulsatile secretion of GnRH, influenced by the SCN , stimulates the secretion of LH, which, in turn, stimulates the production of Te, while Te inhibits the secretion of GnRH and LH [34], thus framing testis-brain inhibitory loop. The cell autonomous pulse-generating mechanism of GnRH secretion plays an important role in Te regulation [35].

Oscillations in Te levels show multi-scale repetitive patterns. Ultraradian harmonics with a period of 1–3 h, depending on the individual, and the circadian rhythm of 24 h are clearly observed [36]; in particular, the Te level typically has a peak value between 7:00 am and 7:30 am [37]. Longer cycles of plasma testosterone levels with periods ranging between 8 and 30 days, with a cluster of periods around 20–22 days have been also reported [38].

Actual biological measurements, including those of hormonal levels, are never periodic in the mathematical sense and display fluctuations. This complex signal shape can be portrayed in two ways: either as a periodic function corrupted by random noise or as a solutions of a nonlinear dynamical system admitting quasi-periodic and chaotic attractors. Chaotic dynamics might underlie normal physiological function, producing no periodicity and being (in some sense) easier to control than periodic rhythms [39]. 2.3 Notably, telling a perturbed periodic solution from a quasiperiodic one from a temporally limited data set is virtually impossible. The discussion regarding the relevance of deterministic chaos to biological oscillation is long-established, e.g. [40], and has been substantiated by experimental evidence [41]. With all the unstable modes accompanying a chaotic attractor, it can be seen as a vehicle to promote adaptation to the environment through exploration of the state space. In both cases, entrainment phenomena are highly relevant and have not been studied previously in hybrid oscillators.

Another complication in discerning rhythms from discrete biological data sets is sampling time [42]. This is a sensitive point in many experimental studies of endocrine systems as blood samples cannot be taken arbitrarily often. There is also a limit on the total amount of blood drawn from an organism. For instance, in studies of Te regulation, 10 min sampling is standard for measuring the concentrations of LH and Te, while an analysis of the closed-loop dynamics rather suggests 1–3 min sampling to capture the relevant transients, see e.g. [43].

1.5. The paper organization

The rest of this review is organized as follows. Section 2 presents a brief review of dynamic models, used to portray circadian clocks. In Section 3, the basic stability and entrainment properties of the classical Goodwin oscillator are considered; its hybrid counterpart used in modeling of endocrine rhythms is also introduced. Section 4 and Section 5 present the results of bifurcation analysis for the continuous and hybrid Goodwin models, respectively. Section 6 concludes the paper.

2. Dynamical models of circadian rhythm

The main circadian oscillator, located at the SCN, is constituted by tens of thousands of interacting neurons; each of them exhibits circadian oscillations, however, their periods may slightly differ. A suitable model for this complex system is therefore a *network* of coupled dynamical systems. Each of the coupled oscillators, corresponding to an individual cell, is expected to exhibit a stable *limit cycle* and be entrainable to periodic external cues.

Mathematical modeling is about approximation and reduction of the underlying phenomena and does not make much sense unless the purpose of modeling is clearly specified. In the biomedical field, a range of models of increasing complexity is needed, to highlight different levels of system organization. Simple models usually lend themselves to analytical methods; this class of model is typically used to study entrainability of circadian rhythms, their effect on endocrine system and other systems of the organism. More complex and detailed models, describing the biochemical mechanisms of circadian clocks in full, usually cannot be examined without recourse to numerical studies. Two questions arise with regard to the circadian oscillator network modeling: First, what is the most appropriate mathematical model for individual clock and, second, how to describe the coupling among them that leads to global entrainment.

2.1. Individual circadian clocks

From a mathematical viewpoint, an oscillator can be defined as a dynamical system whose trajectories are bounded yet do not converge (have non-trivial ω-limit

set); such systems are also referred to as Yakubovich-oscillatory [44–46]. In physics and biology, a more narrow class of oscillators is usually considered, featuring stable limit cycles or at least periodic orbits [9] and thus able to generate self-sustained periodic solutions.

One of the simplest mathematical descriptions of a T-periodic signal is the sine wave

$$x(t) = A\sin(\omega_0 t + \varphi_0), \quad \omega_0 = \frac{2\pi}{T},$$

produced by the second-order linear system

$$\ddot{x}(t) + \omega_0^2 x(t) = 0$$

with circular orbits $\{(x(t), \dot{x}(t))\}$. The intensity of oscillation is determined by the amplitude A, and the quantity φ_0 is called phase shift. With $T = 24\ h$, this model is capable of capturing the periodicity of the circadian rhythms, as well as describing the deviations from the normal LD cycle through positive or negative values of φ_0. From a biological viewpoint, it is reasonable to introduce a bias to the sine wave in order to guarantee non-negativity of the signal

$$x(t) = A(1 + \sin(\omega_0 t + \varphi_0)).$$

The corresponding signal is apparently generated by a third-order linear system. In physical literature, oscillators whose trajectories can be approximated by harmonic signals are sometimes called *quasilinear* [9].

The harmonic oscillator and other linear models have several shortcomings. They do not in particular allow for dynamical interaction within the loop but only describe the effect of an oscillator on another system. Linear oscillators are marginally stable systems, whose trajectories are non-robust to small disturbances, thus posing a risk of numerical issues and solution divergence. Also , the signal shape of the assumed model is not very close to the observed LD-cycles due to day-night variations of light and a nonlinear description of the dynamics has to be introduced in the model to resolve this issue.

For the aforementioned reasons, sustained circadian oscillations are commonly described by nonlinear *limit-cycle* oscillators. One of the simplest systems, exhibiting stable limit cycle, is known as the *Liénard equation* [47]

$$\ddot{x} + f(x)\dot{x} + g(x) = 0, \tag{1}$$

where f and g are continuous function; Usually, f is even $f(x) = f(-x)$ and g is odd $g(x) = -g(-x)$ (in the original work [47], $g(x) = x$). The system (1) may be considered as mass-spring-damper system, where characteristics of the damper and spring are nonlinear. Liénard established conditions on the function $F(x) = \int_0^x f(s)ds$, ensuring the existence and uniqueness of the limit cycle (which, in this case, appears to be exponentially stable). These conditions hold e.g. for the celebrated *van der Pol* oscillator [48], being a special case of (1)

$$\ddot{x} - \mu(1 - x^2)\dot{x} + \omega^2 x = 0. \tag{2}$$

In the case when $0 < \mu << 1$, equation (2) may be considered as a regular perturbation of the usual harmonic oscillator. As one of its applications, van der Pol proposed, in particular, the heartbeat rhythm modeling [49]. In general, Liénard oscillator (1) may have several limit cycles, and estimation of their number remains a challenging problem even for polynomial functions f, g, see [50].

A long-studied problem is the behavior of forced solutions in the perturbed Liénard oscillator

$$\ddot{x} + f(x)\dot{x} + g(x) = Mp(t), \tag{3}$$

where $p(t) = p(t + T)$ stands for an exogenous periodic excitation. It is known that, for some amplitudes $M > 0$, the harmonically disturbed oscillator $p(t) = \sin(\omega t)$ has several periodic solutions, and at least one of them is unstable [51]. For some parameters, a harmonic excitation may lead to unbounded solutions in (3), even though all solutions of the undisturbed (autonomous) system (1) are bounded [52]. A method to study input-to-state stability (ISS) of (1) with respect to $p(\cdot)$ has been proposed in [53], establishing, in particular, the ISS property for the van der Pol model.

With properly tuned parameters, the van der Pol oscillators [54–56] and their interconnections [57] capture many properties of circadian rhythms, in particular, light entrainment. Alternative second-order models for circadian rhythms in *Drosophila* have been introduced by Pavlidis [58]. However, these simple second-order models only mimic the behavior, making the circadian clock "tick", but do not disclose the actual biological mechanism. These mechanisms of sustained oscillations are revealed by more sophisticated *molecular* models.

In their seminal paper [59], Yates and Pardee described a feedback mechanism of *self-regulation* in the metabolic pathway that controls production of pyrimidines in *E. coli* cells and leads to self-sustained oscillations in the metabolites' levels. Later on, a *genetic* feedforward mechanism of *lac* (lactose) *operon* in enteric bacteria was described by Jacob and Monod [11], whose discovery became a breakthrough in genetics and was recognized, along with Lwoff's works on virus synthesis, by the Nobel Prize in physiology and medicine in 1965. In the same year, the seminal model of *Goodwin's oscillator* was proposed [60], being a joint "offspring" of the Yates-Pardee and Jacob-Monod's control circuits and describing a self-sustained generic oscillation in a cell, maintained by inhibitory feedback.

In its classical formulation, Goodwin's model is given by

$$\begin{aligned} \dot{x}_1(t) &= -b_1 x_1(t) + h(x_3(t)), \\ \dot{x}_2(t) &= -b_2 x_2(t) + g_1 x_1(t), \\ \dot{x}_3(t) &= -b_3 x_3(t) + g_2 x_2(t). \end{aligned} \tag{4}$$

The state variables $x_i(t)$, $i = 1, 2, 3$, stand for the concentrations of some chemicals and the constant $b_i > 0$ correspond to their clearing rates. The gains $g_1, g_2 > 0$ and a *non-increasing* nonlinearity $h(\cdot) \geqslant 0$ characterize

the production rates of the chemicals. Typically,

$$\lim_{\xi\to\infty} h(\xi) = \inf_{\xi\geqslant 0} h(\xi) = 0.$$

The nonlinearity $h(\cdot)$ closes the *negative feedback loop* and is often chosen to be the *Hill* function [16]

$$h(\xi) = \frac{a}{1+\mathcal{K}\,\xi^n}, \tag{5}$$

with $a > 0$, $\mathcal{K} > 0$. The Hill exponent $n > 0$ is not necessarily integer, and often interpreted as the cooperativity in ligands' binding to macromolecules [16, 26].

As will be discussed in the next sections, the simple construct of Goodwin's oscillator model has been adopted as a basic modeling paradigm in endocrine systems. It is remarkable that eight year prior to the publication of Goodwin's work, a special case of his model with a piecewise-linear feedback nonlinearity $h(\cdot)$ was proposed in [61] to describe periodic oscillations in the thyroid hormones.

Intuitively, Goodwin's oscillator (4) functions as follows. When the level of Chemical 3 is low, the production rate of Chemical 1 is near its maximum, thus accelerating production of Chemical 2 (since $g_1 > 0$) and, indirectly, Chemical 3 (since $g_2 > 0$). On the other hand, a high concentration of Chemical 3 corresponds to a low production rate of Chemical 1, which also decelerates the production of Chemical 2 and Chemical 3. In [60], Chemicals 1-3 are respectively a gene's mRNA, a protein into which the gene expresses, and an intermediate enzyme, repressing the gene's activity. Later in [62], Goodwin's model has been used to describe testosterone regulation in the male, treating $x_i(t)$ as the blood levels of GnRH, LH and Te hormones; similar models are also used to describe oscillatory metabolic pathways of the Yates-Pardee type [63, 64].

Goodwin reported that the feedback mechanism in (4) may exhibit a stable limit cycle, choosing the Hill function (5) with $n = 1$, which statement proves to be wrong: the equilibrium point of such a system is globally attractive [65, 66]. It was also noticed [67] that Goodwin's oscillator (4),(5) with $n \leqslant 8$ always has a stable equilibrium, whereas the system can have stable periodic orbits for $n > 8$, arising through the Hopf bifurcation. Stability properties of Goodwin's model are discussed in Section 3.

The third (dynamical) order of Goodwin's oscillator is caused by the necessity to have a stable limit cycle (an isolated periodic orbit). Systems of *two* coupled reactions exhibit stable limit cycles only in rare situations, when one of the reactions is auto-catalytic [68], otherwise periodic oscillations are exhibited only when the model has a *center*-type equilibrium, surrounded by a nested family of closed orbits, as in the usual harmonic oscillator [60, 69].

The complete molecular mechanisms of circadian clocks are much more complicated than the Goodwin construct, as demonstrated by the aforementioned models of genetic oscillators in mammals, insects, plants and bacteria [13–15, 17, 70]. Another example is the model of circadian rhythm in cyanobacteria, controlled by the cluster of three genes *kaiA, kaiB, kaiC* and the three corresponding proteins that are coupled by multiple stimulatory and inhibitory feedbacks (the word "kai" is the Japanese for "cycle") [12, 71]. Nevertheless, the third-order Goodwin-like oscillators are often used as "minimal" models of intracellular circadian clocks in studies on entrainment [72–74]. Unlike (4), the reactions' kinetics in these models are typically nonlinear and described by e.g. the Mikhaelis-Menten equations [73, 74]. More important, third-order Goodwin-type models naturally arise via *reduction* of high-order biochemical oscillators, e.g. models of protein phosphorylation in eukaryotes [16].

2.2. Networks of oscillators

Whereas models of circadian clocks accurately describe individual neurons, their synchronization mainly remains a mystery. In reality, neurons communicate via sending out electric pulses, or *stimuli*, of very short length, compared to the oscillation periods. Photoreceptors of the retina also convert light into pulsatile signals, influencing the SCN. To simplify analysis of networked circadian clocks, these pulsatile interactions are often emulated by "averaged" continuous coupling [73, 75–77], depending on the mean-field concentration of a special neurotransmitting peptide (a byproduct of the clock gene's expression); the exogenous signals are also continuous. Extensive numerical simulations reveal [73, 76, 77] that coupling among slightly differing circadian oscillators not only leads to the phase and frequency locking, but also dramatically increases entrainability of the oscillators to exogenous cues.

At the same time, mathematical results on synchronization of Goodwin's oscillators are in fact very limited and primarily deal with *diffusively coupled* oscillators (the coupling is continuous in time and depends on the deviations between the solutions of coupled subsystems) and special interaction graphs (e.g. undirected or balanced). Local criteria for synchronization in such networks can be established by using Master Stability Function (MSF) approach [78]. Non-local synchronization of oscillators is usually proved by using such tools as passivity [79] and its extensions, e.g. convergent dynamics [80] or incremental dissipativity [81–84]. Most of the aforementioned results are restricted to identical oscillators; for heterogeneous networks, only a few global synchronization conditions are known, see e.g. [85, 86]. Characteristics of the collective periodic rhythm in oscillator networks are usually computed by using harmonic balance methods [87–89].

To reduce the complexity of oscillator network models, the actual dynamics of phase oscillators are often replaced by one-dimensional *phases*, evolving on the real line or the unit circle $\mathbb{S}^1$. A tacit assumption adopted in such models is that pulsatile interactions between the individual clocks are rather weak, so the neighbors' stimuli do not drive the oscillator's trajectory away from the stable periodic orbit. The oscillator phase can be imagined as the angular coordinate of the solution along this orbit, and the influence of electric pulses is modeled as the instantaneous jump in the

phase, or *phase resetting*. The magnitude of this jump is phase dependent, that is, the same stimulus affects oscillator differently at different parts of its cycle. The correspondence between the phase and its jump is described by the phase response (resetting) curve (PRC), which can be considered as a counterpart of the impulse response function in linear systems and used as a *control* tool [90–93]. The reader is referred to [91, 93] for the relevant mathematical theory. Zeitgeber signals are also modeled as periodic sequences of pulses, and the influence of each pulse on an oscillator is also described by a PRC map [94, 95]. Hence the ensemble of oscillators is modeled as a complex *hybrid* system [96], which is referred to as the pulse-coupled oscillator (PCO) network and determined by the set of individual PRC maps and an *event-triggered* communication protocol, determining when and how oscillators emit stimuli. PCO networks have attracted serious attention since the publication of seminal work [97], see e.g. [98–108] and references therein. However, even the reduction of the actual circadian pacemaker model to a PCO network does not shed light on synchronization of heterogeneous oscillators: most of the results are confined to synchronization between oscillators with identical natural frequencies.

For this reason, the model complexity is further reduced, replacing the event-triggered pulsatile interactions by the conventional diffusive coupling (mathematically, this reduction relies on averaging techniques [109]). The resulting continuous-time dynamical system is referred to as the *Kuramoto* network [110, 111]

$$\dot\theta_i(t) = \omega_i + \sum_{j=1}^{N} a_{ij} Q(\theta_j(t) - \theta_i(t)), \quad i = 1, \dots, N. \quad (6)$$

Here N stands for the number of oscillators, $\theta_i(t) \in \mathbb{R}$ is the phase of ith oscillator, ω_i is its natural frequency, Q is a periodic function (being a counterpart of the PRC map) and the gains $a_{ij} \geqslant 0$ encode the interaction graph and intensities of interactions between subsystems. Under the assumption of identical frequencies, Kuramoto oscillator networks are closely related to multi-agent consensus algorithms [112, 113]. For a survey of mathematical results, pertaining to Kuramoto networks, and their numerous applications in physics and engineering, the reader is referred to [114–117]. The problem of jet lag, without any relation to the endocrine system, is studied in [24] with respect to the forced Kuramoto oscillator representing the neurons of the SCN in the hypothalamus implementing the circadian clock. The model is shown to explain the differences in recovery from jet lag symptoms due to east-bound and west bound long-distance longitudinal travel.

3. Continuous and Impulsive Goodwin's Models

In this section, basic properties of the continuous Goodwin model given by (4) and its impulsive counterpart are discussed.

3.1. Stability properties of the continuous Goodwin model

Henceforth assume that the function $h : [0, \infty) \to [0, \infty)$ in (4) is C^1*-smooth* and *non-increasing*, i.e. $h'(\xi) \leqslant 0$.

Introducing the state vector $\mathbf{x}(t) = [x_1, x_2, x_3]^T$, (4) is rewritten in a state-space form as

$$\frac{d\mathbf{x}}{dt} = \mathbf{f}(\mathbf{x}) = \mathbf{A}\mathbf{x} + \mathbf{B}h(x_3),$$
$$\mathbf{A} = \begin{bmatrix} -b_1 & 0 & 0 \\ g_1 & -b_2 & 0 \\ 0 & g_2 & -b_3 \end{bmatrix}, \quad \mathbf{B} = \begin{bmatrix} 1 \\ 0 \\ 0 \end{bmatrix}, \quad \mathbf{x}(t) = \begin{bmatrix} x_1(t) \\ x_2(t) \\ x_3(t) \end{bmatrix}. \quad (7)$$

Since $\mathbf{A}$ is Hurwitz and Metzler, the vector $\mathbf{B}$ is non-negative and $h(x_3) \geqslant 0$ for $x_3 \geqslant 0$, the system is easily shown to be *positive*: any solution starting at a nonnegative point $\mathbf{x}(0) \geqslant 0$ (the inequalities apply element-wise) remains non-negative $\mathbf{x}(t) \geqslant 0$. Since $h(x_3)$ is bounded $0 \leqslant h(x_3) \leqslant h(0)$, all such solutions are uniformly bounded and forward complete (exist up to ∞).

The point $\mathbf{x}_*$ is an equilibrium of (4) if and only if $f(\mathbf{x}_*) = 0$, which is equivalent to the system of equations

$$-b_1 x_1^* + h(x_3^*) = g_1 x_1^* - b_2 x_2^* = g_2 x_2^* - b_3 x_3^* = 0$$
$$\Leftrightarrow \begin{cases} x_1^* = \dfrac{b_2}{g_1} x_2^* = \dfrac{b_2 b_3}{g_1 g_2} x_3^*, \quad x_2^* = \dfrac{b_3}{g_2} x_3^*, \\ x_3^* = c\, h(x_3^*), \quad c = \dfrac{g_1 g_2}{b_1 b_2 b_3} > 0. \end{cases} \quad (8)$$

Since the function $h(\cdot)$ is non-increasing, the latter system has the only (non-negative) root $x_3^* \geqslant 0$, corresponding to the unique biologically feasible equilibrium $\mathbf{x}_* \geqslant 0$.

Stability properties of the unique equilibrium are determined by the eigenvalues of the Jacobian

$$\mathbf{Df}(\mathbf{x}_*) = \begin{bmatrix} -b_1 & 0 & h'(x_3^*) \\ g_1 & -b_2 & 0 \\ 0 & g_2 & -b_3 \end{bmatrix}, \quad (9)$$

being the roots of the characteristic equation

$$\begin{aligned} &\det\left(\lambda \mathbf{I} - \mathbf{Df}(\mathbf{x}_*)\right) = \lambda^3 + a_1\lambda^2 + a_2\lambda + a_3 = 0, \\ &a_1 = b_1 + b_2 + b_3 > 0, \\ &a_2 = b_1\, b_2 + b_1\, b_3 + b_2\, b_3 > 0, \\ &a_3 = b_1\, b_2\, b_3 - g_1 g_2 h'(x_3^*) \geqslant b_1\, b_2\, b_3 > 0. \end{aligned} \quad (10)$$

Using the Routh-Hurwitz criterion, the equilibrium of (4) is stable if $\Theta = a_1 a_2 - a_3 < 0$ and unstable when $\Theta > 0$. This leads to the following lemma.

Lemma 1. *If $\mathcal{M}(\xi) = (-\xi h'(\xi)/h(\xi)) < 8$ for any $\xi \geqslant 0$, then the equilibrium is stable for all $b_i, g_i > 0$. If $\sup_{\xi \geqslant 0} \mathcal{M}(\xi) > 8$, the discriminant $\Theta = a_1 a_2 - a_3$ can be both positive and negative, depending on $b_i, g_i > 0$, and the system undergoes an Andronov-Hopf bifurcation as $\Theta = 0$.*

The first part of Lemma 1 follows from the *secant stability criterion* for circulant matrices [118, 119], implying that the Jacobian $\mathbf{Df}(\mathbf{x}_*)$ is Hurwitz if and only if

$$\frac{g_1 g_2 (-h'(x_3^*))}{b_1 b_2 b_3} \overset{(8)}{=} -\frac{x_3^* h'(x_3^*)}{h(x_3^*)} = \mathcal{M}(x_3^*) \leqslant \left(\sec\frac{\pi}{3}\right)^3 = 8.$$

An alternative simpler proof, based on the McLaurin's inequality, is available in [62, 120]. The second part relies on the implicit function theorem and has been proved (for a more general non-cyclic feedback system) in [120, 121].■

Lemma 1 implies the following well-known fact [62, 67].

Corollary 1. *For Goodwin's oscillator in* (4) *with Hill nonlinearity* (5)*, the equilibrium is locally stable whenever* $n \leqslant 8$*. When* $n > 8$*, the system may have unstable equilibrium and undergoes the Hopf bifurcation as* $\Theta = 0$*.*

Indeed, for Hill function (5) one has

$$\mathcal{M}(\xi) = \frac{n\mathcal{K}\xi^n}{a + \mathcal{K}\xi^n} < n = \lim_{\zeta\to\infty} \mathcal{M}(\zeta) \quad \forall \xi \geqslant 0.\blacksquare$$

Note that establishing *global* stability of the equilibrium when $\mathcal{M}(\xi) < 8$ remains a non-trivial problem. Some sufficient conditions are given by the "global" version of the secant criterion [119] and monotonicity-based criteria [65, 66, 122], which imply, in particular, the global stability of the equilibrium for $n = 1$. Simulations show that the same holds for any $n \leqslant 8$, but a proof, to the best of the authors' knowledge, remains elusive. It should be noticed that Corollary 1 is not valid for Goodwin's model with transport delays [123, 124]

$$\begin{aligned} \dot{x}_1(t) &= -b_1 x_1(t) + h(x_3(t-\tau_3)),\\ \dot{x}_2(t) &= -b_2 x_2(t) + g_1 x_1(t-\tau_1),\\ \dot{x}_3(t) &= -b_3 x_3(t) + g_2 x_2(t-\tau_2). \end{aligned} \tag{11}$$

Such a system may have limit cycles for any $n > 1$ (provided that the sum of the delays $\sum_i \tau_i$ is sufficiently large). Detailed analysis of delayed Goodwin's model is beyond the scope of this review; its entrainability properties have not in fact been studied yet.

A fundamental property of Goodwin's oscillator is the existence of a non-trivial periodic orbit in the case when the (unique) equilibrium is unstable.

Theorem 1. *Let the equilibrium* $\mathbf{x}_*$ *be unstable, i.e. the real part of an eigenvalue of* $\mathbf{Df}(\mathbf{x}_*)$ *is positive. Then system* (4) *has a (non-constant) periodic orbit. Furthermore, almost all trajectories converge to closed orbits.*

The proof is based on the seminal result from [125], extending the Poincaré-Bendixsson theory to cyclic systems and implying [126] that the ω-limit set of any bounded solution in (4) can be the equilibrium point, a closed orbit or a homoclinic cycle. A more detailed analysis shows [126] that, in the case of Goodwin's oscillator, homoclinic trajectories are impossible, and hence every solution converges to the equilibrium or a closed orbit. Solutions of the first type span the *stable manifold* of the unstable equilibrium $\mathbf{x}_*$, which is a zero-measure set [127, Proposition 4.1]. ■

Remark 1. *An alternative topological proof of the first statement was published in [128, 129] (and requires some technical assumptions, e.g.* $h(\cdot)$ *being* C^2*-smooth). This proof is based on the existence of an invariant toroidal domain in the vicinity of the equilibrium, enabling one to prove the existence of a periodic orbit by means of the standard method of Poincaré sections. The second statement of Theorem 1 can be proved [120] by using the well-known Yakubovich criterion [45], stating that in a dynamical system with bounded solutions and hyperbolic equilibria almost all solutions oscillate (have non-trivial* ω*-limit sets).*

Notice that Theorem 1 does not establish the uniqueness of a periodic orbit in the Goodwin model and showing uniqueness remains a non-trivial open problem. It is remarkable that the delayed version of Goodwin's oscillator in (11) may have arbitrarily many limit cycles [124].

3.2. Entrainment to periodic signals

Consider now the dynamics of the forced Goodwin's oscillator

$$\begin{aligned} \dot{x}_1(t) &= -b_1 x_1(t) + h(x_3(t)),\\ \dot{x}_2(t) &= -b_2 x_2(t) + g_1 x_1(t),\\ \dot{x}_3(t) &= -b_3 x_3(t) + g_2 x_2(t) + M\beta(t), \end{aligned} \tag{12}$$

that can be rewritten in a matrix form as follows

$$\frac{d\mathbf{x}}{dt} = \mathbf{f}(t,\mathbf{x}) = \mathbf{A}\mathbf{x} + \mathbf{B}h(x_3) + M\mathbf{B_0}\beta(t),$$

where $\mathbf{A}, \mathbf{B}$ are defined in (7) and $\mathbf{B_0} = \begin{bmatrix}0 & 0 & 1\end{bmatrix}^T$. Here $\beta(t) \geqslant 0$ stands for a T_β-periodic function. In the context of endocrine regulation, $M\beta(t)$ corresponds to the signal produced by SCN of the hypothalamus and influencing the secretion of the hypothalamic release hormones, e.g. CRH, GnRH. The phase and, to some extent, the frequency of $\beta(t)$ are controlled by the zeitgebers. This signal may be considered as a feedforward control input to the closed-loop pulsatile endocrine system that modulates the hormone concentrations to an oscillation pattern consistent with the circadian rhythm. Then M stands for the corresponding feedforward gain. Alternatively, M can be considered as the sensitivity of an individual endocrine regulation system ("axis") to circadian rhythm. The analysis below primary deals with the influence of the feedforward control gain $M > 0$ on the behavior of system (12), in particular, the existence and stability of forced periodic solutions. 2.1

Using the Schauder fixed point theorem, the following existence result can be proved [130].

Lemma 1. *Consider system* (12)*, where* $h(\xi) > 0, \forall \xi \geqslant 0$*,* $h'(\cdot)$ *is continuous, and both* h *and* h' *are bounded on* $[0,\infty)$ *(monotonicity of* h *is not required). Then, for any* $M > 0$ *and bounded function* $\beta(t) = \beta(t + T_\beta) \geqslant 0$*,* (12) *has a strictly* positive T_β*-periodic solution.*

Obviously, all T-periodic solutions of (12) are non-constant unless $\beta(\cdot)$ is constant. A natural question arises whether the periodic solution is unique and stable. Both properties can be guaranteed for sufficiently large M, as shown by the following theorem.

Theorem 2. *Let the assumptions of Lemma 1 hold and $h'(\xi) \to 0$ as $\xi \to \infty$, $\beta(t) \geqslant 0$ and $\beta(t) > 0$ on the set of positive measure. Then, for large $M > 0$, the T_β-periodic solution $\mathbf{x}_M(\cdot)$ to (12) is unique and globally attractive.*

The proof of Theorem 2 is based on the following technical lemma, proved in Appendix.

Lemma 2. *Under the assumptions of Theorem 2, there exists a number $\eta > 0$, such that system (12) is convergent (incrementally stable) in the domain $G_\eta = [0, \infty) \times [0, \infty) \times (\eta, \infty) \subset \mathbb{R}^3$ in the following sense: if two solutions $\mathbf{x}(t), \tilde{\mathbf{x}}(t)$ stay in G_η for all $t \geqslant t_0$, then the deviation between them vanishes asymptotically*

$$\lim_{t\to\infty} |\mathbf{x}(t) - \tilde{\mathbf{x}}(t)| = 0. \tag{13}$$

To prove Theorem 2, we are going to show first that, for large M, every solution $\mathbf{x}(t)$ of the system (12) arrives at the set G_η defined in Lemma 2 and stays there for large t. Consider the T_β-periodic solution of the linear system

$$\frac{d\mathbf{x}^+}{dt} = \mathbf{A}\mathbf{x}^+ + \mathbf{B_0}\beta(t), \quad \mathbf{x}^+(t) = \mathbf{x}^+(t + T_\beta).$$

As demonstrated in [84], such a solution is unique:

$$\mathbf{x}^+(t) = \int_0^\infty e^{s\mathbf{A}}\mathbf{B_0}\beta(t-s)ds = \int_{-\infty}^t e^{(t-s)\mathbf{A}}\mathbf{B_0}\beta(s)ds. \tag{14}$$

Moreover, this solution is strictly uniformly positive since the vector $e^{s\mathbf{A}}\mathbf{B_0}$ is positive for any $s \geqslant 0$ and thus the integrand is positive on a set of positive measure. In particular, $x_3^+(t) \geqslant \varkappa > 0$, where $\varkappa$ depends only on $\beta(\cdot)$ and the parameters b_i, g_i in (12) but not on M and $h(\cdot)$.

Consider now an arbitrary solution $\mathbf{x}(\cdot)$ to (12) and notice that the function $\zeta(t) = \mathbf{x}(t) - M\mathbf{x}^+(t)$ satisfies the equation

$$\dot{\zeta}(t) = \mathbf{A}\zeta(t) + \mathbf{B}h(x_3(t)).$$

1.1 Recalling that $\forall t : h(x_3(t)) > 0$, $\mathbf{A}$ is a Hurwitz, and the function $e^{s\mathbf{A}}\mathbf{B}$ is positive, one shows that

$$\varliminf_{t\to\infty} \zeta_3(t) \geqslant 0,$$

entailing that $\varliminf_{t\to\infty} x_3(t) \geqslant M\varkappa$. Choosing $M > \eta/\varkappa$ and recalling that $x_1(t), x_2(t) \geqslant 0$ in view of the system's positivity, results in $\mathbf{x}(t) \in G_\eta$ for t sufficiently large.

Now Lemma 2 implies that (13) holds for any two solutions $\mathbf{x}(t), \tilde{\mathbf{x}}(t)$. In particular, the T_β-periodic trajectory is unique and globally attractive.■

Remark 2. *The uniqueness part of Theorem 2 remains valid for a more general class of nonlinearities that actually can be unbounded; The corresponding proof inspired by the techniques from [131] can be found in [84]. Notice however that this approach does not allow to prove global stability. The idea of the proof presented above was communicated to the authors by Dr. Denis Efimov. Theorem 2 remains valid for any non-negative matrix $\mathbf{B}_0 \neq 0$ and vector function $\beta(t) = \beta(t+T_\beta) \geqslant 0$ of appropriate dimension, ensuring thus the Goodwin's model entrainment by arbitrary multidimensional periodic cues.*

The general results of Lemma 1 and Theorem 2 remain valid for many positive nonlinear systems, different from Goodwin's oscillator, e.g. "repressilators" and "promotilators" [132]. In view of Lemma 1, the forced system has a periodic solution even when the equilibrium of autonomous system (4) ($M = 0$) is stable; the solution $x_M(t)$ is then also stable for small M. If the equilibrium of (4) is unstable, the periodic solution of (12) is usually also unstable for small $M > 0$ (unless T_β coincides with the free-running period, $\mathbf{x}_M(t)$ is close to the equilibrium $\mathbf{x}_*$ as $M \to 0$).

Notice that the critical amplitude M_0, beyond which the uniqueness and stability of the periodic orbit is ensured by Theorem 2, can be explicitly estimated, but the estimate is very conservative. At the same time, Theorem 2 gives no clue regarding the character of the system's solutions for small amplitudes of M. Simulations, presented in Section 4 for the case of a harmonic signal $\beta(t)$, demonstrate that, for small M, the system exhibits quasiperiodic behavior, arising via the secondary Hopf (torus) bifurcation as the T_β-periodic cycle looses its stability.

3.3. Goodwin-type models of endocrine regulation

The original paradigm of Goodwin's oscillator, i.e. (4) and (5), fits well into the simplified structure of Te regulation in the male, with the concentration of the three hormones constituting the axis GnRH-LH-Te assigned to be the state variables. The concentration of Te exhorts negative feedback on the concentration of GnRH through $h(x_3)$ by inhibiting its release. Similarly, the regulation of cortisol can also be cast within the same structure but for the axis CRH-ACTH-cortisol, e.g. with Michaelis-Menten degradation kinetics in the hypothalamic, pituitary, and adrenal regions to avoid the use of unrealistically high Hill coefficients necessary for oscillation in the classical model, [133]. Goodwin's oscillator is often called the Smith model [62] in the context of endocrine regulation.

Being a conceptual (phenomenological) model, Goodwin's oscillator, in its classical form, neither necessarily fits experimental data nor captures in detail the underlying biological mechanisms. In the endocrine regulation of Te, a significant modelling difficulty is presented by the fact that GnRH secretion by the hypothalamic neurons is not continuous but rather episodic. In fact, synchronized GnRH neurons collectively produce bursts of hormone concentration [134], whose amplitude and frequency are dependent on the concentration of Te. This pulse-modulated mechanism has been established experimentally [135] and implements a negative feedback as the amplitude and frequency of the GnRH pulses decrease.

To bring Goodwin's oscillator (the Smith model) in agreement with the compelling biological evidence, the

original static nonlinear feedback $h(\cdot)$ in (12) is substituted with a frequency-amplitude pulse modulation mechanism in [43, 136]. The resulting model is termed the impulsive Goodwin's oscillator. It possesses hybrid dynamics as the feedback is implemented by pulse modulation of the first kind [137] and thus introduces a first-order discrete subsystem into the closed loop of the oscillator. The state of the forced continuous part is given by

$$\frac{d\mathbf{x}}{dt} = \mathbf{A}\mathbf{x} + M\mathbf{B_0}\beta(t), \tag{15}$$

where $x_1(t)$ undergoes jumps at the time instants t_k, $k \geqslant 0$

$$x_1(t_k^+) = x_1(t_k^-) + \lambda_k, \quad t_{k+1} = t_k + T_k,$$

whose timing and magnitudes are specified by the amplitude and frequency modulation functions

$$\lambda_k = F(x_3(t_k)), \quad T_k = \Phi(x_3(t_k)).$$

The superscripts "$-$" and "$+$" denote the left- and right-side limits, respectively. A distinctive property of the impulsive Goodwin's oscillator is absence of equilibria that resolves the issue with convergent (non-oscillatory) trajectories in the continuous Goodwin model [43]. Along with boundedness of the solutions [43], it agrees well with the original biological function of producing oscillatory temporal patterns. Furthermore, a rich diversity of signal shapes (hormone concentration profiles) can be achieved by varying the pulse modulator nonlinearities $\Phi(\cdot)$ and $\Psi(\cdot)$. Even without time delay, the impulsive Goodwin's oscillator can exhibit multiple periodic solutions of different periods, as well as deterministic chaos [138].

4. Bifurcation analysis of the continuous Goodwin model

In this section, we study nonlinear dynamics of Goodwin's oscillator, in its autonomous mode as well as subject to exogenous force, by means of bifurcation analysis.

4.1. Autonomous Goodwin's oscillator

Fig. 1 and Fig. 2 exemplify the behaviors of the classical Goodwin's oscillator given by (4),(5). Fig. 1a depicts the Andronov-Hopf bifurcation for $n = 9$ producing the oscillatory dynamics. For $b_1 < b_1^L$, the system possesses a stable equilibrium $\mathbf{x}_*$. For this parameter interval (Fig. 2), Jacobian (9) has a pair of complex-conjugated eigenvalues $\lambda_{1,2} = \mu \pm i\omega$ with negative real parts $\mu < 0$, and one negative real eigenvalue $\lambda_3 < 0$. At the point $b_1 = b_1^L$, the equilibrium state undergoes an Andronov-Hopf bifurcation. As illustrated in Fig. 1b, when the parameter b_1 passes through the value $b_1 = b_1^L$, a pair of complex-conjugated eigenvalues $\lambda_{1,2} = \mu \pm i\omega$ crosses the imaginary axis into the positive real half-plane. As a result, the equilibrium state becomes unstable, and a stable limit cycle appears. With further increase in the value of b_1, the unstable equilibrium point undergoes a reverse Andronov-Hopf bifurcation at the point $b_1 = b_1^R$, in which a stable limit cycle turns into a stable equilibrium state (Figs. 1a,b). In the bifurcation diagram Fig. 1a, the oscillatory state exhibits maximum and minimum values in the temporal variation of the state variable x_3. The maximum and minimum values of the state variable x_3 correspond to the points, where phase trajectories intersect the surface $S = \{\mathbf{x} : g_2x_2 - b_3x_3 = 0\}$ in the phase space of system (4),(5) from the two directions (two-sided Poincaré map). Fig. 2a shows a two-dimensional projection of the phase portrait for a stable equilibrium point $\mathcal{O}$ ($n = 8$). Fig. 2b–d illustrate two-dimensional projections of the phase portrait for $n = 9, 12, 14$ after the Andronov-Hopf bifurcation, where the equilibrium point becomes unstable. Here C denotes a stable limit cycle and $\mathcal{O}_*$ is the unstable equilibrium point.

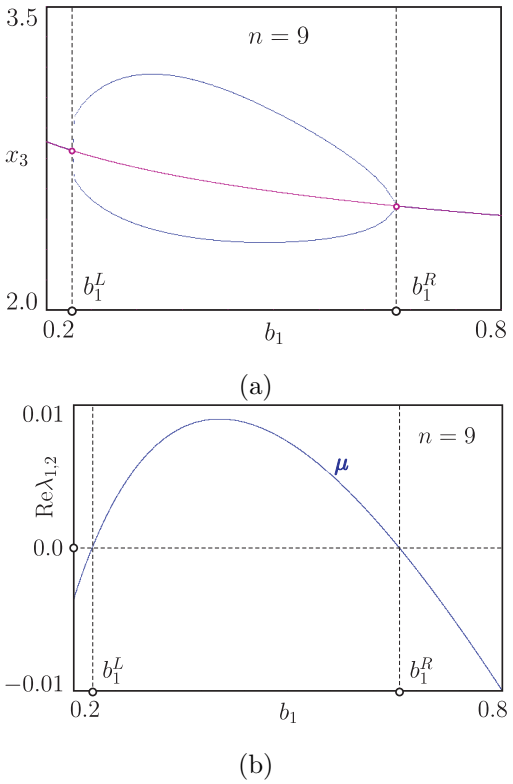

Figure 1: Birth of a limit cycle from a stable equilibrium point in an Andronov-Hopf bifurcation. $n = 9$, $b_2 = 0.5$, $b_3 = 0.3$, $g_1 = 2.0$, $g_2 = 0.5$, $a = 100$, $\mathcal{K} = 0.1$ and $0.2 < b_1 < 0.8$. (a) Bifurcation diagram. b_1^L and b_1^R are the Andronov-Hopf bifurcation points. (b) Variation of the real part $\mathrm{Re}\lambda_{1,2} = \mu$ of eigenvalues $\lambda_{1,2} = \mu \pm i\omega$. Note that $\lambda_3 < 0$.

4.2. Forced oscillations

Consider the forced Goodwin's oscillator in (12) with the Hill nonlinearity (5), subject to a positive single-tone harmonic exogenous signal (i.e. the linear oscillator portraying circadian rhythm) $\beta(t) = 1 + \sin(\omega t + \theta)$ of the period $T_\beta = 2\pi/\omega$.

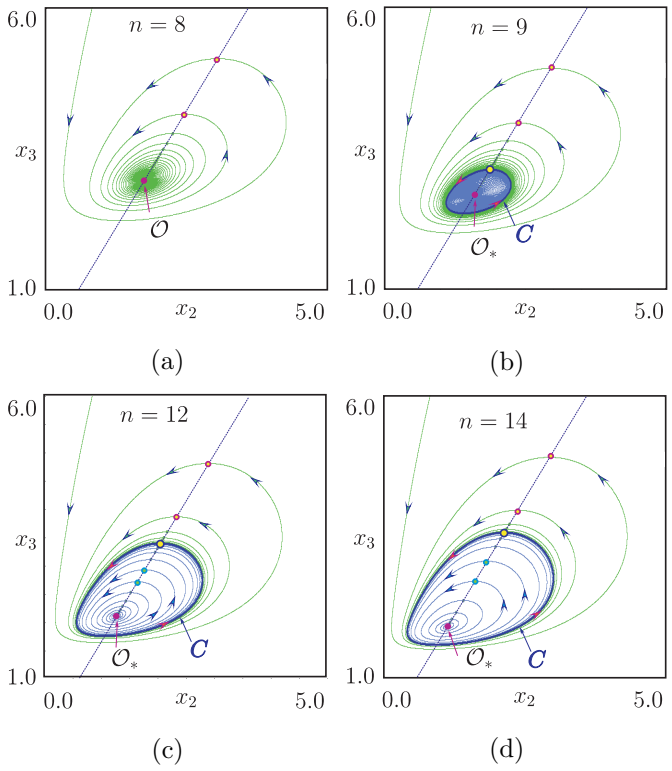

Figure 2: Phase portraits dynamical system (4),(5) for different values of n; $b_1 = 0.4$, $b_2 = 0.5$, $b_3 = 0.3$, $g_1 = 2.0$, $g_2 = 0.5$, $a = 100$, $\mathcal{K} = 0.1$. (a) $n = 8$, $\mathcal{O}$ is the stable equilibrium point. (b)-(d) Two-dimensional projection of the phase portrait for $n = 9$, $n = 12$ and $n = 14$, respectively. Here $\mathcal{O}_*$ is the unstable equilibrium point surrounded by the stable limit cycle C. The maximum value of x_3 corresponds to the points where phase trajectories intersect the surface $S = \{\mathbf{x} : g_2 x_2 - b_3 x_3 = 0\}$ in the state space (1) in the one direction (Poincaré map).

For the analysis, the parameters are chosen as $n = 9$, $a = 100$ $\mathcal{K} = 0.1$, $b_1 = 0.4$, $b_2 = 0.5$, $b_3 = 0.3$, $g_1 = 2.0$, $g_2 = 0.5$, $0 < M < 0.055$, $T_\beta = 2\pi/\omega = 1440$, $\theta = 0$.

A period-T_β solution $\mathbf{x}_M(t)$ of (12) corresponds to the fixed point of the stroboscopic map $\mathbf{x}(t) \mapsto \mathbf{x}(t + T_\beta)$. The fixed point of this map is located using the Newton-Raphson algorithm that allows not only to evaluate stable cycles but also unstable ones. To test stability of the periodic solutions, one computes the eigenvalues ρ_1, ρ_2, ρ_3 (henceforth $|\rho_1| \geqslant |\rho_2| \geqslant |\rho_3|$) of the monodromy matrix $\Phi(T_\beta)$ that satisfies

$$\frac{d\Phi(t)}{dt} = \mathbf{Df}(t, \mathbf{x}_M)\Phi(t), \quad \Phi(0) = I.$$

Fig. 3a shows a one-dimensional bifurcation diagram calculated for $0 < M < 0.055$ and constructed from a Poincaré section in the phase space of (12). For large amplitudes M of the forcing signal $\beta(t)$, (12) exhibits a stable period-T_β solution. As M is reduced, this solution undergoes an Andronov-Hopf bifurcation (or a Neimark-Sacker bifurcation for the fixed point in the corresponding Poincaré map), and loses stability when the absolute value of the complex-conjugate multipliers $|\rho_1| = |\rho_2|$ becomes greater than one.

The variation of $\rho_{1,2}$ as a function of the amplitude M is shown in Fig. 3b. The pair of complex-conjugate multipliers leaves the unit circle at a point $M = M_\varphi$. The loss of cycle stability leads to the soft appearance of two-frequency quasiperiodic oscillations corresponding to a two-dimensional invariant torus T_q in the phase space of (12), and the intersection of T_q with the Poincaré section corresponds to the closed invariant curve C_a of the Poincaré map. Fig. 3c presents the phase portrait of (12) after the Andronov-Hopf bifurcation for $M = 0.035$.

As emphasized in Sec. 3.1, autonomous system (4),(5) has no periodic orbits for $n \leqslant 8$. Simulation shows that the forced continuous Goodwin's oscillator in (12) exhibits only a period-T_β solution for $n \leqslant 8$ (see Fig. 3d).

5. Circadian entrainment of the impulsive Goodwin's oscillator

Consider a solution $\mathbf{x}(t)$ to (15). Due to linearity of the continuous part of the model, it can be written as $\mathbf{x}(t) = \mathbf{x}_p(t) + \mathbf{B_0}\vartheta(t)$, where $\mathbf{x}_p(t)$ is governed by

$$\frac{d\mathbf{x}_p}{dt} = \mathbf{A}\mathbf{x}_p(t), \quad \mathbf{x}_p(t_k^+) = \mathbf{x}_p(t_k^-) + \lambda_k \mathbf{B}, \tag{16}$$

and $\vartheta(t)$ satisfies

$$\dot{\vartheta}(t) = -b_3\vartheta(t) + M\beta(t).$$

In the interval $t_k \leqslant t < t_{k+1}$, the solution to system (16) is given by

$$\mathbf{x}_p(t) = \mathrm{e}^{\mathbf{A}(t-t_k)}\mathbf{x}_p(t_k^+), \tag{17}$$

with

$$\mathbf{x}_p(t_k^+) = \mathbf{x}_p(t_k^-) + \lambda_k \mathbf{B}. \tag{18}$$

Substituting (18) into (17) yields

$$\mathbf{x}_p(t) = \mathrm{e}^{\mathbf{A}(t-t_k)}(x_p(t_k^-) + \lambda_k \mathbf{B}). \tag{19}$$

For $t = t_{k+1}$, the solution above has the form

$$\begin{aligned} \mathbf{x}_p(t_{k+1}^-) &= \mathrm{e}^{\mathbf{A}\,(t_{k+1}-t_k)}(\mathbf{x}_p(t_k^-) + \lambda_k \mathbf{B}), \\ t_{k+1} &= t_k + \Phi(x_3(t_k^-)), \quad \lambda_k = F(x_3(t_k^-)). \end{aligned} \tag{20}$$

In this way, the evolution of continuous-time system (15) through the jump points t_k is as follows [139]

$$\mathbf{x}_p(t_{k+1}^-) = Q_p(\mathbf{x}_p(t_k^-), t_k), \tag{21}$$

where the discrete map Q_p is defined by

$$\begin{aligned} Q_p(\mathbf{x}_p(t_k^-), t_k) &= \mathrm{e}^{\mathbf{A}T_k}(\mathbf{x}_p(t_k^-) + \lambda_k \mathbf{B}), \\ T_k &= \Phi(x_3(t_k^-)(t_k)), \quad \lambda_k = F(x_3(t_k^-)). \end{aligned}$$

To simplify the index notation, rename the components of the continuous state vector $\mathbf{x}_p(t) = [x(t), y(t), z(t)]^T$.

Since $x_3(t) = z(t) + \vartheta(t)$, then

$$t_{k+1} = t_k + \Phi(z(t_k^-) + \vartheta(t_k)), \; \lambda_k = F(z(t_k^-) + \vartheta(t_k)).$$

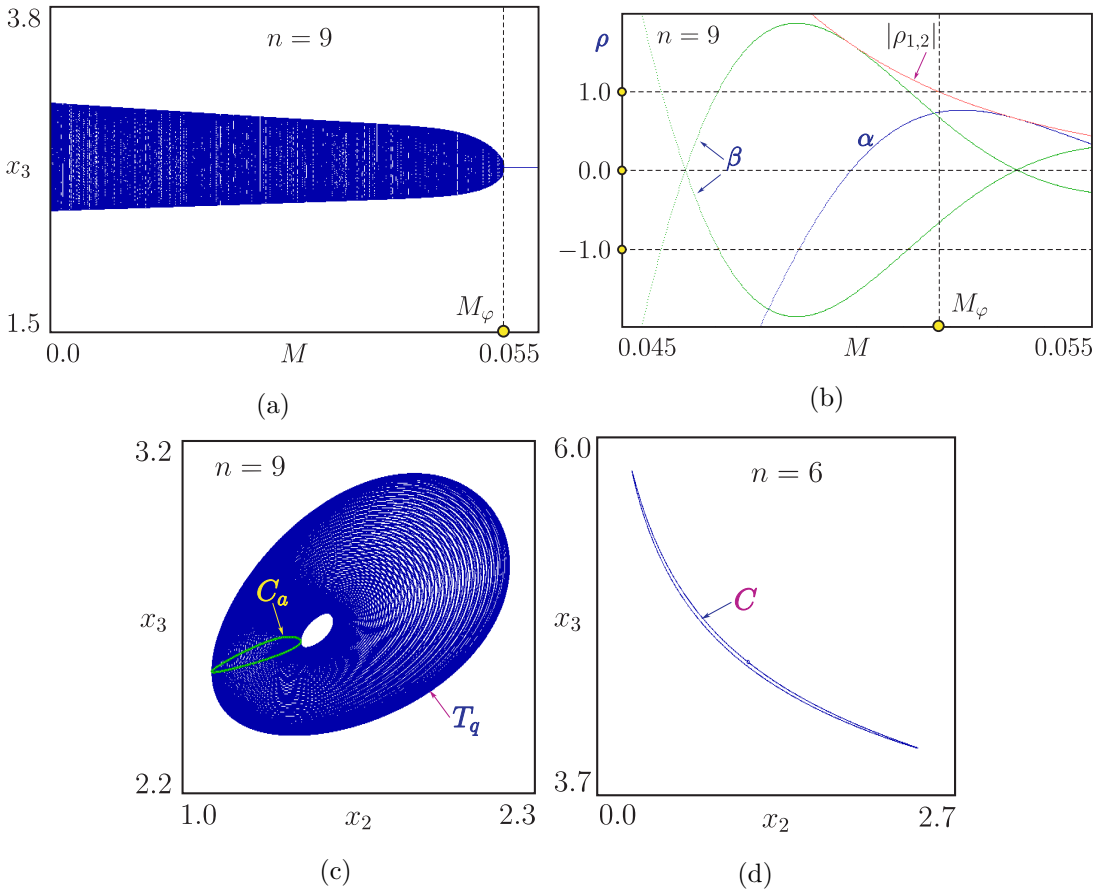

Figure 3: Periodic and quasi-periodic solutions in continuously forced Goodwin's oscillator: (a) Bifurcation diagram illustrating the appearance of the two-dimensional torus through a Andronov-Hopf bifurcation. $b_1 = 0.4$, $b_2 = 0.5$, $b_3 = 0.3$, $g_1 = 2.0$, $g_2 = 0.5$, $a = 100$, $\mathcal{K} = 0.1$, $n = 9$, $0.0 < M < 0.055$. M_φ is the bifurcation point. (b) Multiplier diagrams for the stable 1-cycle, $0.045 < M < 0.055$. As the parameter M decreases, a pair of complex-conjugated multipliers $\rho_{1,2} = \alpha \pm i\beta$ of the 1-cycle leave the unit circle at the point $M = M_\varphi$. (c) Two-dimensional projection of the phase portrait after the Andronov-Hopf bifurcation for $M = 0.035$. Here T_q is the two-dimensional torus associated with the quasiperiodic solution of (12) and C_a denotes a closed invariant curve C_a of the corresponding Poincaré map. (d) Two-dimensional projection onto the plan (x_2, x_3) of the period-T_β solution for $n = 6$ and $M = 0.6$.

Here $\vartheta(t) = \frac{M}{b_3^2+\omega^2}\left[b_3 \sin(\omega t + \theta) - \omega \cos(\omega t + \theta)\right] + \frac{M}{b_3}$.

Introduce $\varphi = \omega t$ and $x(t_k^-) = x_k$, $y(t_k^-) = y_k$, $z(t_k^-) = z_k$, $\varphi(t_k) = \varphi_k$. In this way $\varphi_{k+1} = \varphi_k + \Phi(z_k + \vartheta(\varphi_k))$ and $\lambda_k = F(z_k + \vartheta(\varphi_k))$. Then the Poincaré map of the forced model in (15) can be rewritten as [139]

$$
\begin{aligned}
x_{k+1} &= \mathrm{e}^{-b_1 T_k}(x_k + \lambda_k), \qquad (22)\\
y_{k+1} &= E_{21}(T_k)(x_k + \lambda_k) + \mathrm{e}^{-b_2 T_k} y_k,\\
z_{k+1} &= E_{31}(T_k)(x_k + \lambda_k) + E_{32}(T_k) y_k + \mathrm{e}^{-b_3 T_k} z_k,\\
\varphi_{k+1} &= \varphi_k + \omega\, T_k \pmod{2\pi}, \quad k = 0, 1, 2, ...,
\end{aligned}
$$

with

$$
\begin{gathered}
T_k = \Phi(\sigma_k), \quad \lambda_k = F(\sigma_k),\\
\sigma_k = z_k + \frac{M}{b_3^2+\omega^2}\left[b_3 \sin(\varphi_k + \theta) - \omega \cos(\varphi_k + \theta)\right] + \frac{M}{b_3},\\
0 \leqslant \varphi_k \leqslant 2\pi, \quad 0 \leqslant \theta \leqslant 2\pi,\\
E_{21}(T) = \frac{g_1}{b_2 - b_1}(\mathrm{e}^{-b_1 T} - \mathrm{e}^{-b_2 T}),\\
E_{32}(T) = \frac{g_2}{b_3 - b_2}(\mathrm{e}^{-b_2 T} - \mathrm{e}^{-b_3 T}),\\
E_{31}(T) = \alpha_1 \mathrm{e}^{-b_1 T} + \alpha_2 \mathrm{e}^{-b_2 T} + \alpha_3 \mathrm{e}^{-b_3 T},\\
\alpha_1 = \frac{g_1 g_2}{(b_2 - b_1)(b_3 - b_1)}, \quad \alpha_2 = \frac{g_1 g_2}{(b_1 - b_2)(b_3 - b_2)},\\
\alpha_3 = \frac{g_1 g_2}{(b_1 - b_3)(b_2 - b_3)}.
\end{gathered}
$$

The modulation functions of the intrinsic pulsatile feedback are selected as

$$
\Phi(\sigma) = k_1 + k_2 \frac{(\sigma/r)^n}{1 + (\sigma/r)^n}, \quad F(\sigma) = k_3 + \frac{k_4}{1 + (\sigma/r)^n}.
$$

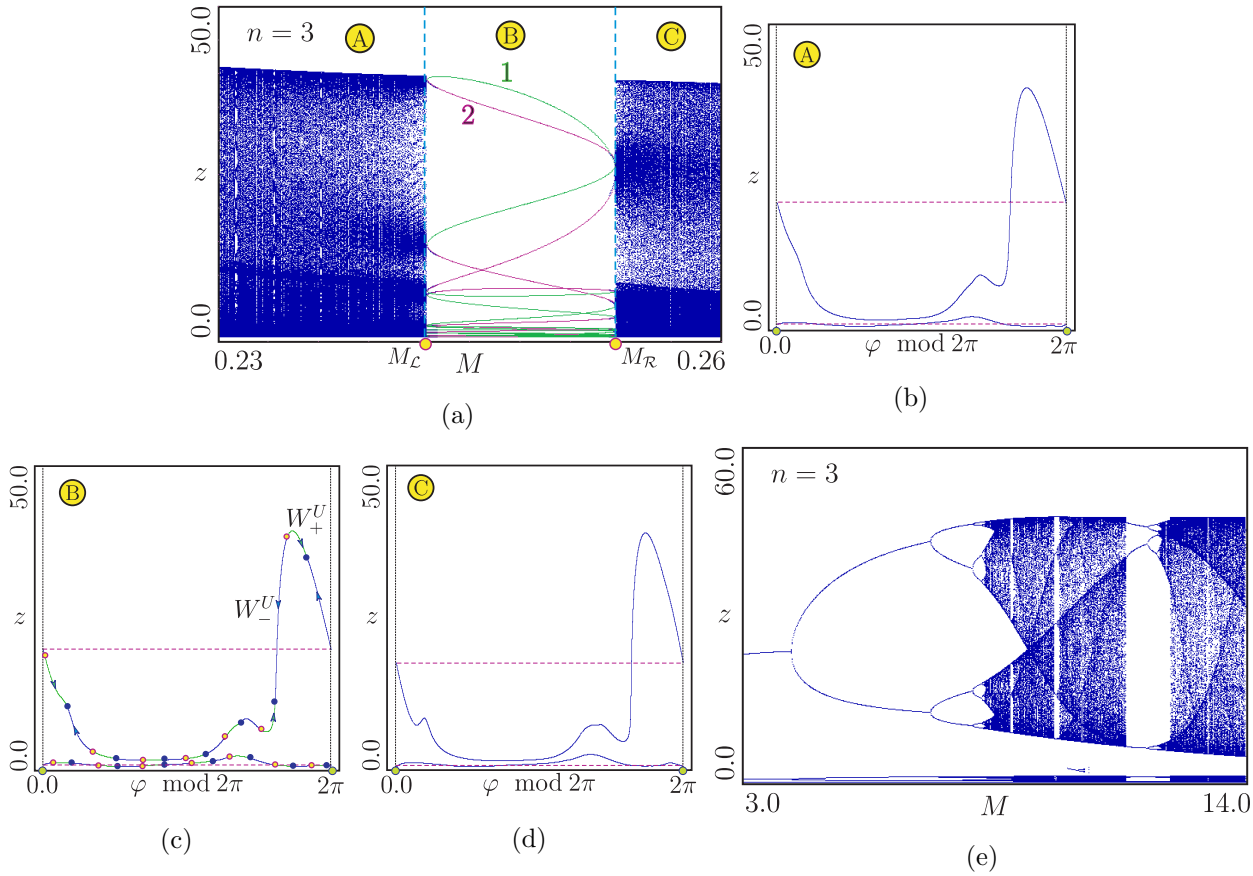

Figure 4: The impulsive Goodwin's oscillator: (a) Bifurcation diagram for $0.23 \leqslant M \leqslant 0.26$ illustrating a transition from quasiperiodic to periodic dynamics and vice versa in a saddle-node bifurcation at $M_{\mathcal{L}}$ and $M_{\mathcal{R}}$. $b_1 = 0.45$, $n = 3$. (b) Phase portrait of the map before the saddle-node bifurcation for $M = 0.242$. (c) Phase portrait of the map after the saddle-node bifurcation. $M = 0.246$. Here, solid circles mark the stable 14-cycle and open circles mark the saddle ones. $W^U_{\pm}$ are unstable manifolds of the saddle 14-cycle. (d) Phase portrait of the map after the saddle-node bifurcation at $M = M_{\mathcal{R}}$. $M = 0.2546$. (e) Bifurcation diagram for large values of M illustrating a period-doubling transition to chaos, $3.0 \leqslant M \leqslant 14.0$.

The introduction of the exogenous signal β modifies the argument of the modulation function and can be effectively interpreted as time-dependence of $F(\cdot)$ and $\Phi(\cdot)$. Actually, from a solution to (22), it is impossible to tell whether $\beta(t)$ exerts effect on the closed-loop dynamics through an additive contribution to the continuous part of (15) or directly alters the modulation functions. The latter fact is meaningful since important properties of the impulsive Goodwin's oscillator, such as intrinsic boundedness of the solutions, are preserved in the forced version of the model. Yet, compared to the autonomous case, bistability appears in the forced system dynamics, [139]. Another crucial observation is that $\sigma_k \geqslant x_k$ due to the positivity of the exogenous signal. Since the modulation functions $F(\cdot)$ and $\Phi(\cdot)$ are bounded from below and above, the modulation depth is reduced by $\beta \geqslant 0$ thus resulting in a smaller range of λ_k, T_k.

5.1. Bifurcation analysis

The parameter values are selected as: $0.0 \leqslant M \leqslant 12.0$, $0.23 < b_1 < 0.69$, $b_2 = 0.014$, $b_3 = 0.15$, $g_1 = 0.6$, $g_2 = 1.5$, $k_1 = 50$, $k_2 = 220.0$, $k_3 = 1.5$, $k_4 = 5.0$, $r = 2.7$, $n = 3$. In the following analysis, the amplitudes of the forcing signal M and b_1 are used as the bifurcation parameters.

For a relatively small amplitude M, map (22) displays a quasiperiodic orbit. As M increases, the system enters the 1:7 entrainment region (or phase-locked region) via a saddle-node bifurcation at the point $M_{\mathcal{L}}$. This transition is shown in Fig. 4a for $b_1 = 0.45$. On the part of the bifurcation diagram in Fig. 4a that falls to the left of the point $M_{\mathcal{L}}$, map (22) has a stable closed invariant curve, associated with quasiperiodic dynamics, as illustrated in Fig. 4b. The saddle-node bifurcation at the edge of the entrainment region produces a new attracting closed invariant curve (Fig. 4c). This closed curve includes two 14-cycles, a saddle and stable node, and is formed by the saddle-node connection composed of the unstable manifolds $W^U_{\pm}$ of the saddle cycle. In this way, inside the entrainment region, map (22) has the stable and saddle 14-cycles. The green lines in Fig. 4a (marked with 1) represent the saddle 14-cycle and the magenta lines (marked with 2) represent the stable 14-cycle.

When crossing the saddle-node bifurcation point $M_{\mathcal{R}}$ with increasing amplitude M of the forcing signal, the sta-

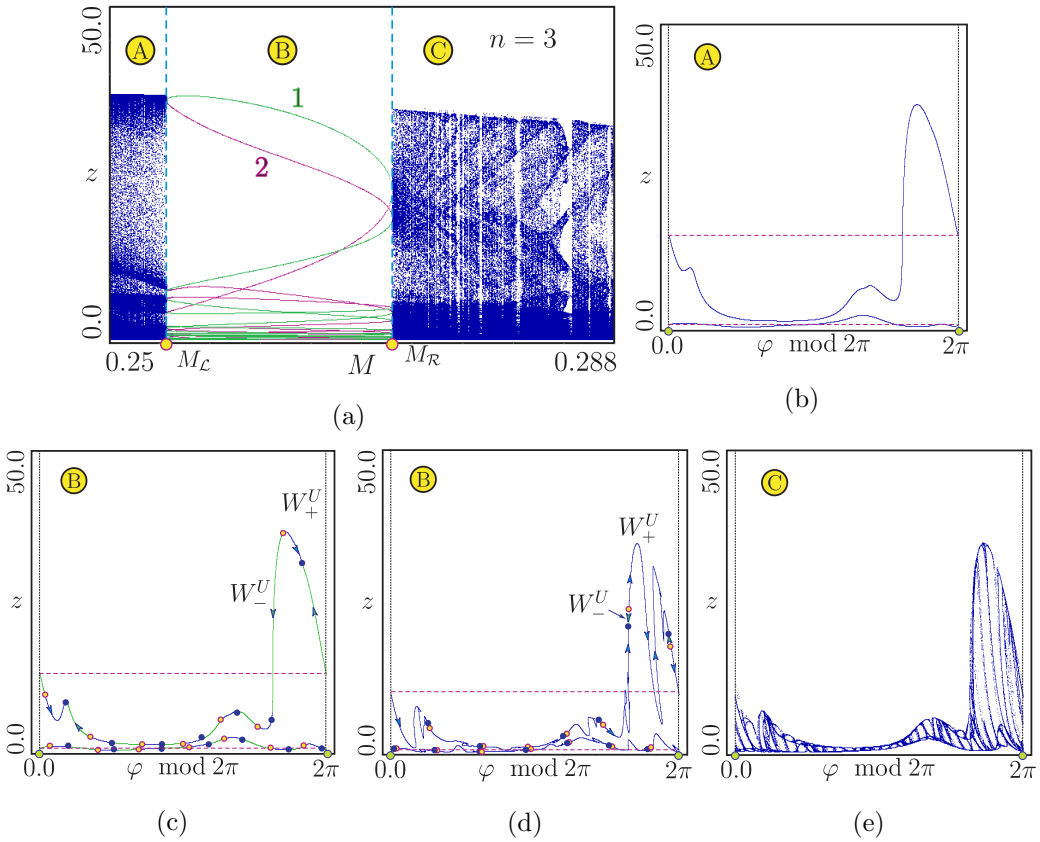

Figure 5: (a) Bifurcation diagram showing the transition from a quasiperiodic orbit to a period-14 resonant dynamics in a saddle-node bifurcation with subsequent transition to a chaotic attractor through loss of smoothness and destruction of the invariant curve. $0.25 \leqslant M \leqslant 0.288$. $b_1 = 0.5$, $n = 3$. (b) Phase portrait of the map before the saddle-node bifurcation at $M_{\mathcal{L}}$. $M = 0.252$. (c) Phase portrait of the map after the saddle-node bifurcation. $M = 0.258$. Here, solid circles mark the stable 14-cycle and open circles mark the saddle ones. $W_{\pm}^U$ are unstable manifolds of the saddle 14-cycle. (d) Phase portrait of the map near the second saddle-node bifurcation at $M_{\mathcal{R}}$, $M = 0.27116$. (e) Phase portrait of the map when the system lives the entrainment region (after the destruction of the closed invariant curve). $M = 0.0.27325$.

ble 14-cycle merges with the saddle one and disappears. As one can see in Figs. 4c,d, the saddle-node bifurcation at $M_{\mathcal{R}}$ leads to the appearance of the stable closed invariant curve, associated with quasiperiodic dynamics (Fig. 4d). The one-dimensional bifurcation diagram in Fig. 4e shows a period-doubling transition to chaos for large M.

Fig. 5 shows another example of a bifurcation transition in which a stable closed curve is destroyed when leaving the 1:7 entrainment region for $b_1 = 0.5$. The destruction of a stable closed invariant curve typically leads to the appearance of a chaotic attractor [140, 141].

As already mentioned, within each entrainment region (tongue of periodicity), there is a closed invariant curve that is formed by the unstable manifold of the saddle cycle and the points of the stable and saddle cycles.

As one can see in Fig. 5a–c, the transition from a stable closed invariant curve (Fig. 5b), associated with quasiperiodic dynamics, to the closed curve with a periodic attractor (see Fig. 5c) takes place via a saddle-node bifurcation occurring at $M_{\mathcal{L}}$ in the same way as in the example discussed above (see Fig. 4).

However, by contrast to the previous example, with further increase of the forcing signal amplitude M, the invariant curve loses its smoothness at the points of the stable node 14-cycle due to folding of the unstable manifold W_+^U of the saddle 14-cycle (Fig. 5d) and, at the right edge $M_{\mathcal{R}}$ of the entrainment region, transforms to a folded set [142]. This leads to the destruction of the closed curve [140]. Finally, leaving the entrainment region, the saddle and stable node 14-cycles merge and disappear through a saddle-node bifurcation at $M_{\mathcal{R}}$. This bifurcation creates a chaotic attractor (Fig. 5e).

Recall that the saddle-node bifurcation points $M_{\mathcal{L}}$ and $M_{\mathcal{R}}$ define the edges of the the entrainment region (resonance tongue).

Fig. 6a displays a one-dimensional bifurcation diagram for $b_1 = 0.65$ and $0.27 < M < 0.38$, illustrating period-doubling cascades, multistability, and chaotic dynamics.

By contrast to the previous examples (see Fig. 4 and Fig. 5), the transition to period-7 entrainment region $M_{\mathcal{L}} < M < M_{\mathcal{R}}$ takes place via a subcritical period-doubling bifurcation occurring at $M = M_{\mathcal{L}}$. Note that the subcritical period-doubling bifurcation at the left edge $M_{\mathcal{L}}$ of the entrainment region produces a stable node 7-cycle (denoted by 2 in Fig. 6a) and a saddle-14 cycle.

When the system leaves the entrainment region $M_{\mathcal{L}} <$

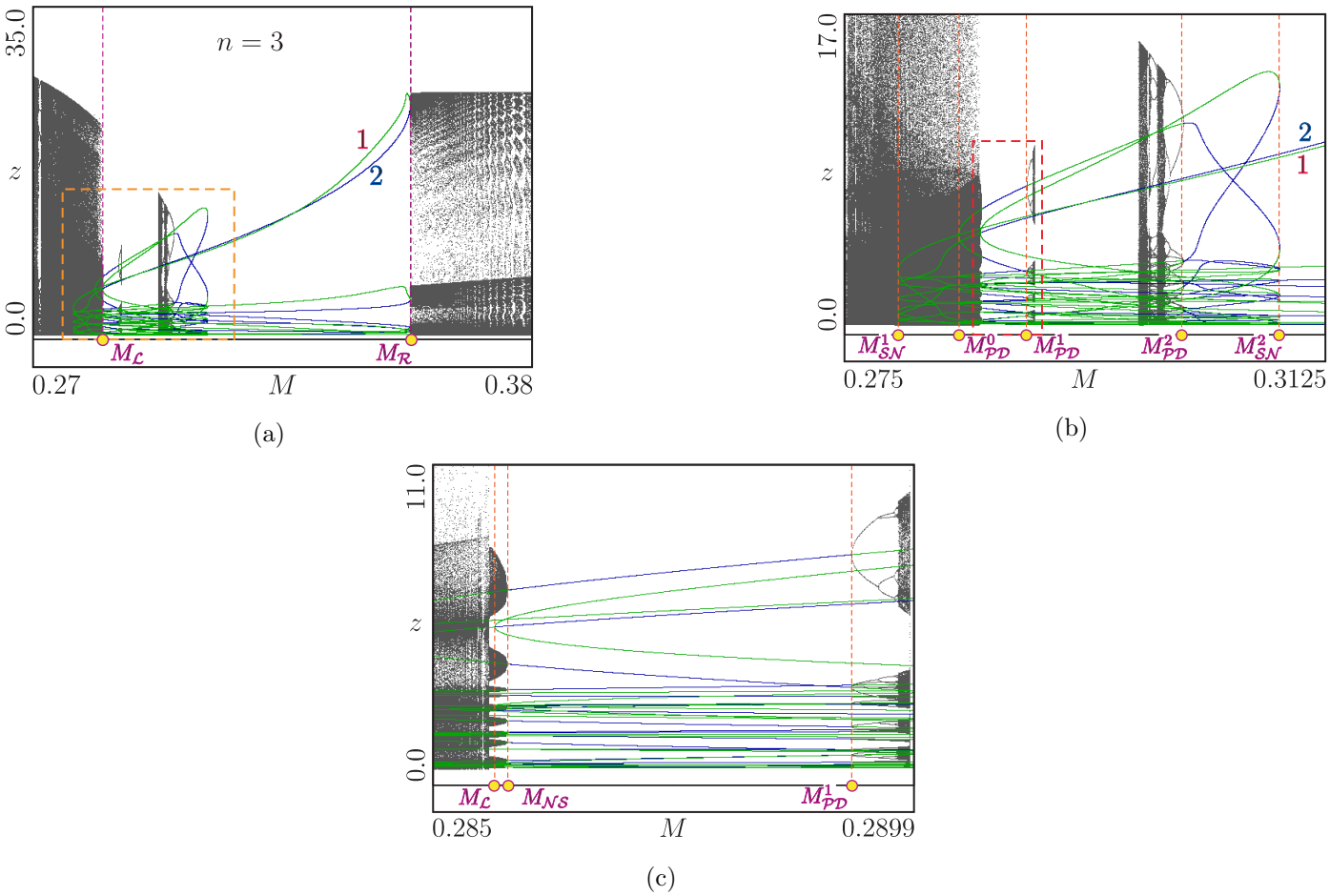

Figure 6: (a) Bifurcation diagram for $b_1 = 0.65$, illustrating multistability and chaotic dynamics in the period-7 entrainment region $M_{\mathcal{L}} < M < M_{\mathcal{R}}$. The line marked by 1 represents the saddle 7-cycle and the line denoted by 2 represents the stable 7 cycle. Here $M_{\mathcal{L}}$ is the reverse subcritical period-doubling bifurcation point for 7-cycle and $M_{\mathcal{R}}$ is the saddle-node bifurcation point for 7-cycle. (b) Magnified part of the bifurcation diagram that is outlined by the rectangle in (a). Here $M^1_{\mathcal{SN}}$, $M^2_{\mathcal{SN}}$ are the fold bifurcation points for 7- and 14-cycles, respectively and $M^{1,2}_{\mathcal{PD}}$ are the supercritical period-doubling bifurcation points for 14-cycles. $M^0_{\mathcal{PD}}$ is the period-doubling bifurcation point for the unstable 7-cycle. (c) Magnified part of the bifurcation diagram in (b). Here $M_{\mathcal{NS}}$ is the Neimark-Sacker bifurcation point for 14-cycle.

$M < M_{\mathcal{R}}$ through the boundary $M_{\mathcal{R}}$, the stable node 7-cycle and saddle 7-cycle merge and disappear in a saddle-node bifurcation. This bifurcation leads to the appearance of a chaotic attractor.

Fig. 6b shows a magnified part of the bifurcation diagram that is outlined by the rectangle in Fig. 6a. Fig. 6c is a magnification of the rectangle outlined in Fig. 6b. The domain between the points of subcritical period-doubling bifurcation $M_{\mathcal{L}}$ and of saddle-node bifurcation M^2_{SN} is a region of multistability, where the stable 7-cycle (denoted by 2) coexists with chaotic or quasiperiodic and stable high-periodic attractors.

Now consider the characteristics of the bifurcational behavior depicted in Fig. 6a and Fig. 6b in more detail in order to understand the mechanism behind the appearance of the coexisting attractors.

As the parameter M increases (see Fig. 6b), two unstable 7-cycles appear through a fold bifurcation at $M = M^1_{SN}$. As already mentioned, when the parameter M passes the value $M = M_L$, the first unstable 7-cycle undergoes a period-doubling bifurcation. The original unstable 7-cycle turns into the stable 7-cycle (denoted by 2), and the saddle 14-cycle appears (Fig. 6b,c).

With further increase of the parameter M, the saddle 14-cycle, which has appeared from the unstable 7-cycle as a results of a subcritical period-doubling bifurcation at $M = M_{\mathcal{L}}$ (see Fig. 6c), merges with the stable 14-cycle and disappears in a saddle-node bifurcation at $M = M^2_{\mathcal{SN}}$ (Fig. 6b).

As illustrated in Fig. 6b, when the parameter M decreases from the value $M^2_{\mathcal{SN}}$, one can observe an infinite cascade of period-doubling bifurcations, leading finally to a transition to chaos. In this way, there exists a region of bistability where where the stable 7-cycle coexists with the chaotic and high periodic attractors.

Finally, as the parameter M increases, the second unstable 7-cycle, which has appeared at $M = M^1_{\mathcal{SN}}$ in a fold bifurcation, undergoes a supercritical period-doubling bifurcation at $M^0_{\mathcal{PD}}$ (see Fig. 6c). This bifurcation leads to the appearance of an unstable 14-cycle and unstable

7-cycle (denoted by 1 in Fig. 6b).

With further increase in the value of M, the unstable 14-cycle becomes a stable one via a reverse Neimark-Sacker bifurcation at $M = M_{\mathcal{NS}}$ (Fig. 6c). Hereafter, when crossing the point M^1_{PD} with increasing M, an infinite cascade of period-doubling bifurcations is observed once again, leading to a transition to chaos (Fig. 6c).

Between the point of the Neimark-Sacker bifurcation $M_{\mathcal{NS}}$ and the point M^1_{PD} of the period-doubling bifurcation, the stable period-7 cycle coexists with the stable 14-cycle.

Note that when crossing the Neimark-Sacker bifurcation point $M_{\mathcal{NS}}$ with decreasing M, the stable 14-cycle turns into an unstable focus 14-cycle. As a result, a stable 14-cyclic closed invariant curve, associated with a quasiperiodic dynamics softly arises from the stable 14-cycle (Fig. 6c). The domain between the points of subcritical period-doubling bifurcation $M_{\mathcal{L}}$ and of Neimark-Sacker bifurcation $M_{\mathcal{NS}}$ in Fig. 6c is a region of bistability, where the stable 7-cycle coexists with the quasiperiodic attractor.

6. Conclusions

Mathematical theory of entrainment and synchronization is mathematically challenging and, being applied to biological oscillators, of fundamental importance for understanding how the circadian rhythm impacts physiological regulation. In particular, the effects of circadian rhythm on the endocrine system, controlling the basic organism functions such as metabolism and reproduction, are especially significant due to their implication in widespread medical condition, e.g. diabetes and cancer.

Constructing a tractable mathematical model of a biological oscillator with a sufficient for the end-purpose realism is a task that demands qualified and coordinated efforts of biologists, mathematicians, as well as engineers. The present paper overviews a number of models developed along this research avenue. The dynamics of two harmonically forced models of Goodwin's oscillator are studied by means of bifurcation analysis with emphasis on entrainment phenomena. In the classical continuous model, quasiperiodic solutions are discovered for small amplitudes of the exogenous signal that, in an Andronov-Hopf bifurcation, become periodic with an increase in the amplitude. Hybrid dynamics lead to much more complex scenarios in the case of the impulsive Goodwin's oscillator, where periodic solutions are observed for moderate values of the exogenous signal, while small and high amplitudes of it can
2.3 result in quasiperiodicity or deterministic chaos. These simulation results can be validated in biological experiments but demand high-resolution hormone concentration data over several days in a row to be conclusive.

Another characteristic phenomenon appearing in the forced impulsive Goodwin's oscillator is the transitions from phase-locked dynamics to quasiperiodicity and chaos that are controlled by the phase of the exogenous signal. The latter property is presumably related to the changes in the endocrine system due to the jet lag.

The transitions from phase-locked periodic dynamics to quasiperiodicity and vice versa are first described in a saddle node bifurcation. Further, it is demonstrated how a stable closed invariant curve loses its smoothness at the point the stable cycle due to folding of the unstable manifold of the saddle cycle as when leaving the entrainment region. This leads to the destruction of the closed curve and appearance of a chaotic attractor.

Appendix A. Appendix. Proof of Lemma 2

The proof of Lemma 2 is based on the seminal idea of *convergent dynamics* (or incremental stability), originating from works by B.P. Demidovich and T. Yoshizawa [80]. We start with the following proposition.

Proposition 1. *Consider a convex set $G \subseteq \mathbb{R}^n$ and the mapping $f : [0,\infty) \times G \to \mathbb{R}^n$. Suppose that $f(t,\mathbf{x})$ has a continuous partial derivative $\frac{\partial}{\partial \mathbf{x}} f(t,\mathbf{x})$ at any point $(t,\mathbf{x}) \in [0,\infty) \times G$ and there exists a matrix $P = P^\top$ such that*

$$P\frac{\partial f(t,\mathbf{x})}{\partial \mathbf{x}} + \frac{\partial f(t,\mathbf{x})}{\partial \mathbf{x}}^\top P \leq -\alpha I_n \quad \forall t \geqslant 0, \mathbf{x} \in G. \quad \text{(A.1)}$$

Then for any $t \geqslant 0$, $\mathbf{x}_0, \mathbf{x}_1 \in G$ the inequality holds

$$2(\mathbf{x}_1 - \mathbf{x}_0)^\top P\left[f(t,\mathbf{x}_1) - f(t,\mathbf{x}_0)\right] \leqslant -\alpha|\mathbf{x}_1 - \mathbf{x}_0|^2. \quad \text{(A.2)}$$

In the special case $G = \mathbb{R}^n$, Proposition 1 has been proved in [80] (see the proof of Theorem 1), the general case is proved in the same way. The principal requirement is convexity of G, entailing that for any $\mathbf{x}_0, \mathbf{x}_1 \in G$ and $s \in [0,1]$ one has $\mathbf{x}_s = s\mathbf{x}_1 + (1-s)\mathbf{x}_0 \in G$, and therefore

$$f(t,\mathbf{x}_1) - f(t,\mathbf{x}_0) = \int_0^1 \frac{\partial}{\partial s} f(t,\mathbf{x}_s) ds = \\ = \int_0^1 \frac{\partial f}{\partial \mathbf{x}}(t,\mathbf{x}_s)(\mathbf{x}_1 - \mathbf{x}_0) ds.$$

Multiplying the latter equality by $(\mathbf{x}_1 - \mathbf{x}_0)^\top P$, one obtains

$$2(\mathbf{x}_1 - \mathbf{x}_0)^\top P(f(t,\mathbf{x}_1) - f(t,\mathbf{x}_0)) = \\ = 2(\mathbf{x}_1 - \mathbf{x}_0)^\top \left(\int_0^1 P\frac{\partial f}{\partial \mathbf{x}}(t,\mathbf{x}_s) ds\right)(\mathbf{x}_1 - \mathbf{x}_0) = \\ = (\mathbf{x}_1 - \mathbf{x}_0)^\top \int_0^1 P\left(\frac{\partial f}{\partial \mathbf{x}}(t,\mathbf{x}_s) + \frac{\partial f}{\partial \mathbf{x}}(t,\mathbf{x}_s)^\top P\right) ds (\mathbf{x}_1 - \mathbf{x}_0) \\ \overset{\text{(A.1)}}{\leq} -\alpha|\mathbf{x}_1 - \mathbf{x}_0|^2. \blacksquare$$

Corollary 2. *Let the assumptions of Proposition 1 be valid and $P = P^\top > 0$. Then the following ODE*

$$\dot{\mathbf{x}}(t) = f(t,\mathbf{x}(t))$$

is convergent in G in the following sense: any two solutions $\mathbf{x}_1(t), \mathbf{x}_2(t)$ that are well-defined and stay in G for $t \geqslant t_0 \geqslant 0$ converge to each other in the sense that

$$|\mathbf{x}_1(t) - \mathbf{x}_2(t)| \xrightarrow[t\to\infty]{} 0,$$

and the convergence is exponentially fast.

The proof of Corollary 2 is immediate from Proposition 1, introducing the Lyapunov function $V(\mathbf{x}_1, \mathbf{x}_2) = (\mathbf{x}_1 - \mathbf{x}_2)^\top P(\mathbf{x}_1 - \mathbf{x}_2)$. Choosing $\varepsilon > 0$ so small that $\varepsilon P < \alpha I_n$ and applying (A.2), one arrives at

$$\frac{d}{dt}V(\mathbf{x}_1, \mathbf{x}_2) = 2(\mathbf{x}_2 - \mathbf{x}_1)^\top P(f(t, \mathbf{x}_2) - f(t, \mathbf{x}_1)) \leq \overset{(A.2)}{\leq} -\varepsilon V(\mathbf{x}_1, \mathbf{x}_2).$$

Since $P > 0$, this implies exponentially fast vanishing of the deviation $|\mathbf{x}_1(t) - \mathbf{x}_2(t)|$ as $t \to \infty$.■

We are now ready to prove Lemma 2. It suffices to show that for sufficiently large $\eta > 0$ the system (12) satisfies the conditions of Corollary 2 for $G = G_\eta$ (obviously, this set is convex). Recall that the matrix $\mathbf{A}$ from (7) is Hurwitz. Hence, a matrix $P = P^\top > 0$ exists such that

$$P\mathbf{A} + \mathbf{A}^\top P \leqslant -2I_3.$$

By assumption, $h'(\xi) \to 0$ as $\xi \to 0$. Therefore, for η sufficiently large one has $(P\tilde{\mathbf{B}} + \tilde{\mathbf{B}}^\top P)h'(\xi) < I_3$ whenever $\xi > \eta$; here $\tilde{\mathbf{B}} = (0, 0, 1)\mathbf{B}$. By noticing that

$$\frac{\partial}{\partial \mathbf{x}} f(t, \mathbf{x}) = \mathbf{A} + \tilde{\mathbf{B}}h'(x_3),$$

one shows that for large $\eta > 0$ the inequality (A.1) holds with $\alpha = 1$ whenever $t \geqslant 0$ and $\mathbf{x} \in G_\eta$, which ends the proof in view of Corollary 2.■

List of Acronyms

ACTH adrenocorticotropin hormone

CRH corticotropin-releasing hormone

GnRH gonadotropin-releasing hormone

ISS input-to-state stability

LD light-dark

LH luteinizing hormone

MSF Master Stability Function

PCO pulse-coupled oscillator

PRC phase response (resetting) curve

SCN suprachiasmatic nucleus

Te testosterone

References

[1] The 2017 nobel prize in physiology or medicine, Nobel Assembly at Karolinska Institutet, online at https://www.nobelprize.org/nobel_prizes/medicine/laureates/2017/press.html.

[2] T. A. Bargiello, M. W. Young, Molecular genetics of a biological clock in Drosophila, Proceedings of the National Academy of Sciences 81 (7) (1984) 2142–2146.

[3] P. Hardin, J. Hall, M. Rosbash, Feedback of the Drosophila period gene product on circadian cycling of its messenger rna levels, Nature 343 (1990) 536–540.

[4] P. Emery, W. So, M. Kaneko, J. C. Hall, M. Rosbash, CRY, a Drosophila clock and light-regulated cryptochrome, is a major contributor to circadian rhythm resetting and photosensitivity, Cell 95 (5) (1998) 669–679.

[5] C. Ibáñez, Scientific background discoveries of molecular mechanisms controlling the circadian rhythm, online at https://www.nobelprize.org/nobel_prizes/medicine/laureates/2017/advanced-medicineprize2017.pdf (2017).

[6] K. Whitehead, M. Pan, K. Masumura, R. Bonneau, N. S. Baliga, Diurnally entrained anticipatory behavior in Archaea, PLoS ONE 4 (5) (2009) e5485.

[7] J. de Mairan, Observation botanique, Hist. Acad. Roy. Sci. (1729) 35–36.

[8] A. de Candolle, Physiologie Végétale, Bechet Jeune, Paris, 1832.

[9] A. Pikovsky, M. Rosenblum, J. Kurths, Synchronization: A Universal Concept in Nonlinear Science, Cambridge University Press, New York, 2001.

[10] R. J. Konopka, S. Benzer, Clock mutants of Drosophila melanogaster, Proceedings of the National Academy of Sciences of the USA 68 (1971) 2112–2116.

[11] F. Jacob, J. Monod, Genetic regulatory mechanisms in the synthesis of proteins, J. Mol. Biol. 3 (1961) 318–356.

[12] G. Kurosawa, K. Aihara, Y. Iwasa, A model for the circadian rhythm of cyanobacteria that maintains oscillation without gene expression, Biophys. J. 91 (6) (2006) 2015–2023.

[13] N. Dalchau, S. J. Baek, H. M. Briggs, F. C. Robertson, A. N. Dodd, M. J. Gardner, M. A. Stancombe, M. J. Haydon, G.-B. Stan, J. M. Gonçalves, A. A. R. Webb, The circadian oscillator gene GIGANTEA mediates a long-term response of the Arabidopsis thaliana circadian clock to sucrose, Proceedings of the National Academy of Sciences 108 (12) (2011) 5104–5109.

[14] J.-C. Leloup, A. Goldbeter, Toward a detailed computational model for the mammalian circadian clock, PNAS 100 (12) (2003) 7051–7056.

[15] D. B. Forger, C. S. Peskin, A detailed predictive model of the mammalian circadian clock, PNAS 100 (25) (2003) 14806–14811.

[16] D. Gonze, W. Abou-Jaoude, The Goodwin model: Behind the Hill function, PLoS One 8 (8) (2013) e69573.

[17] J.-P. Comet, G. Bernot, A. Das, F. Diener, C. Massot, A. Cessieux, Simplified models for the mammalian circadian clock, Procedia Computer Science 11 (2012) 127 – 138, proceedings of the 3rd International Conference on Computational Systems-Biology and Bioinformatics.

[18] K. L. Toh, C. R. Jones, Y. He, E. J. Eide, W. A. Hinz, D. M. Virshup, L. J. Ptáček, Y.-H. Fu, An hper2 phosphorylation site mutation in familial advanced sleep phase syndrome, Science 291 (5506) (2001) 1040–1043.

[19] Y. Xu, K. Toh, C. Jones, J.-Y. Shin, Y.-H. Fu, L. J. Ptáček, Modeling of a human circadian mutation yields insights into clock regulation by PER2, Cell 128 (1) (2006) 59–70.

[20] M. Hatori, S. Gill, L. S. Mure, M. Goulding, D. D. M. O'Leary, S. Panda, Lhx1 maintains synchrony among circadian oscillator neurons of the SCN, eLife 3 (2014) e03357.

[21] E. E. Benarroch, Suprachiasmatic nucleus and melatonin, Neurology 71 (8) (2008) 594–598.

[22] T. A. Wang, Y. V. Yu, G. Govindaiah, X. Ye, L. Artinian, T. P. Coleman, J. V. Sweedler, C. L. Cox, M. U. Gillette, Circadian

rhythm of redox state regulates excitability in suprachiasmatic nucleus neurons, Science 337 (6096) (2012) 839–842.
[23] M. Y. Bothwell, M. U. Gillette, Circadian redox rhythms in the regulation of neuronal excitability, Free Radical Biology and Medicine 119 (2018) 45 – 55.
[24] Z. Lu, K. Klein-Cardena, S. Lee, T. M. Antonsen, M. Girvan, E. Ott, Resynchronization of circadian oscillators and the east-west asymmetry of jet-lag, Chaos 26 (9).
[25] A. M. Vosko, C. S. Colwell, A. Y. Avidan, Jet lag syndrome: circadian organization, pathophysiology, and management strategies, Nat Sci Sleep 2 (2010) 1179–1608.
[26] J. Murray, Mathematical biology, I: An introduction (3rd ed.), Springer, New York, 2002.
[27] L. S. Farhy, Modeling of oscillations in endocrine networks with feedback, Methods in Enzymology 384 (2004) 54–81.
[28] J. Veldhuis, Pulsatile hormone secretion: Mechanisms, significance and evaluation, in: D. Lloyd, E. Rossi (Eds.), Ultradian Rhythms from Molecules to Mind, Springer, Dordrecht, 2008, pp. 229–248.
[29] W. B. Cannon, Organization for physiological homeostasis, Physiol Rev 9 (1929) 399–431.
[30] D. M. Keenan, J. D. Veldhuis, Pulsatility of hypothalamo-pituitary hormones: A challenge in quantification, Physiology 31 (2016) 34–50.
[31] K. L. Gamble, R. Berry, S. J. Frank, M. E. Young, Circadian clock control of endocrine factors, Nat Rev Endocrinol. 10 (8) (2014) 466–475.
[32] S. Chan, M. Debono, Replication of cortisol circadian rhythm: New advances in hydrocortisone replacement therapy, Therapeutic Advances in Endocrinology and Metabolism 1 (3) (2010) 129–138.
[33] M. Bailey, R. Silver, Sex differences in circadian timing systems: Implications for disease, Frontiers in neuroendocrinology 35 (1) (2014) 111–139.
[34] J. D. Veldhuis, Recent insights into neuroendocrine mechanisms of aging of the human male hypothalamic-pituitary-gonadal axis, Journal of Andrology 20 (1) (1999) 1–18.
[35] R. Tsutsumi, N. J. Webster, GnRH pulsatility, the pituitary response and reproductive dysfunction, Endocr J. 56 (6) (2009) 729–737.
[36] S. K. Gupta, E. A. Lindemulder, G. Sathyan, Modeling of circadian testosterone in healthy men and hypogonadal men, The Journal of Clinical Pharmacology 40 (2000) 731–738.
[37] M. J. Diver, K. E. Imtiaz, A. M. Ahmad, J. P. Vora, W. D. Fraser, Diurnal rhythms of serum total, free and bioavailable testosterone and of shbg in middle-aged men compared with those in young men, Clinical Endocrinology 58 (2003) 710–717.
[38] C. H. Doering, H. C. Kraemer, H. K. Brodie, D. A. Hamburg, A cycle of plasma testosterone in the human male, The Journal of Clinical Endocrinology and Metabolism 40 (3) (1975) 492–500.
[39] L. Glass, Synchronization and rhythmic processes in physiology, Nature 410 (2001) 277–284.
[40] L. Glass, M. C. Mackey, From clocks to chaos, Princeton University Press, 1988.
[41] G. N. Derry, P. S. Derry, Characterization of chaotic dynamics in the human menstrual cycle, Nonlinear Biomedical Physics 4 (5). doi:10.1186/1753-4631-4-5.
[42] F. Yates, L. Yates, Ultradian rhythms as the dynamic signature of life, in: D. Lloyd, E. Rossi (Eds.), Ultradian Rhythms from Molecules to Mind, Springer, Dordrecht, 2008, pp. 249–260.
[43] A. Churilov, A. Medvedev, A. Shepeljavyi, Mathematical model of non-basal testosterone regulation in the male by pulse modulated feedback, Automatica 45 (1) (2009) 78–85.
[44] V. Yakubovich, Frequency conditions of oscillations in nonlinear control systems with one single-valued or hysteresis-type nonlinearity, Autom. Remote Control 36 (12) (1975) 1973–1985.
[45] A. Pogromsky, T. Glad, H. Nijmeijer, On diffusion driven oscillations in coupled dynamical systems, Int. J. Bifurcation and Chaos 9 (04) (1999) 629–644.
[46] D. Efimov, A. Fradkov, Oscillatority of nonlinear systems with static feedback, SIAM Journal on Control and Optimization 48 (2) (2009) 618–640.
[47] A. Liénard, Etude des oscillations entretenues, Revue Générale de lElectricité 23 (1928) 901–912 & 946–954.
[48] B. van der Pol, On relaxation oscillations, The London, Edinburgh and Dublin Phil. Mag. & J. of Sci. 2 (7) (1926) 978–992.
[49] B. Van der Pol, J. Van der Mark, The heartbeat considered as a relaxation oscillation, and an electrical model of the heart, Philos. Mag. 6 (1928) 763–775.
[50] F. Dumortier, D. Panazzolo, R. Roussarie, More limit cycles than expected in Liénard equations, Proc. Amer. Math. Society 135 (6) (2007) 1895–1904.
[51] P. Ponzo, Forced oscillations of the generalized Liénard equation, SIAM J. Appl. Math. 15 (1) (1967) 75–87.
[52] T. Burton, C. Townsend, On the generalized Liénard equation with forcing term, J. Differential Equations 4 (1968) 620–633.
[53] D. Angeli, D. Efimov, Characterizations of input-to-state stability for systems with multiple invariant sets, IEEE Transactions on Automatic Control 60 (12) (2015) 3242–3256.
[54] M. Jewett, D. Forger, R. Kronauer, Revised limit cycle oscillator model of human circadian pacemaker, J. Biol. Rhythms 14 (6) (1999) 493–500.
[55] M. Jewett, D. Forger, R. Kronauer, Quantifying human circadian pacemaker response to brief, extended, and repeated light stimuli over the phototopic range, J. Biol. Rhythms 14 (6) (1999) 501–515.
[56] E. Brown, Y. Choe, H. Luithardt, C. Czeisler, A statistical model of the human core-temperature circadian rhythm, Amer. J. Physiol. Endocrinol. Metabolism 279 (2000) E669E683.
[57] K. Rompala, R. Rand, H. Howland, Dynamics of three coupled van der Pol oscillators with application to circadian rhythms, Commun. Nonlin. Sci. Numer. Simulation 12 (5) (2007) 794–803.
[58] T. Pavlidis, W. Kauzmann, Toward a quantitative biochemical model for circadian oscillators, Arch. Biochem. Biophys. 132 (1969) 338–348.
[59] R. Yates, A. Pardee, Control of pyrimidine biosynthesis in Escherichia Coli by a feedback mechanism, J. Biol. Chem. 221 (1956) 757–770.
[60] B. C. Goodwin, Oscillatory behavior in enzymatic control processes, in: G. Weber (Ed.), Advances of Enzime Regulation, Vol. 3, Pergamon, Oxford, 1965, pp. 425–438.
[61] L. Danziger, G. Elmergreen, Mathematical models of endocrine systems, Bull. Math. Biophys. 19 (1957) 9–18.
[62] W. R. Smith, Hypothalamic regulation of pituitary secretion of lutheinizing hormone—II Feedback control of gonadotropin secretion, Bull. Math. Biol. 42 (1980) 57–78.
[63] R. Costalat, J. Burger, Effect of enzyme organization on the stability of Yates-Pardee pathways, Bull. Math. Biol. 58 (4) (1996) 719–737.
[64] S. Doubabi, Study of oscillations in a particular case of Yates-Pardee-Goodwin metabolic pathway with coupling, Acta Biotheoretica 46 (1999) 311–319.
[65] D. J. Allwright, A global stability criterion for simple control loops, Journal of Mathematical Biology 4 (1977) 363–373.
[66] G. Enciso, E. Sontag, On the stability of a model of testosterone dynamics, J. Math. Biol. 49 (6) (2004) 627–634.
[67] J. S. Griffith, Mathematics of cellular control processes. i. negative feedback to one gene., Journal of Theoretical Biology 20 (1968) 202–208.
[68] J. Tyson, Biochemical oscillations, in: C. Fall, E. Marlang, J. Wagner, J. Tyson (Eds.), Computational Cell Biology, Springer, 2004, Ch. 9, pp. 230–260.
[69] L. Danziger, G. Elmergreen, The thyroid-pituitary homeostatic mechanism, Bull. Math. Biophys. 18 (1956) 1–13.
[70] J.-C. Leloup, D. Gonze, A. Goldbeter, Limit cycle models for circadian rhythms based on transcriptional regulation in Drosophila and Neurospora, J. Biol. Rhythms 14 (6) (1999) 433–448.

[71] F. Miyoshi, Y. Nakayama, K. Kaizu, H. Iwasaki, M. Tomita, A mathematical model for the Kai-protein-based chemical oscillator and clock gene expression rhythms in cyanobacteria, J. Biol. Rhythms 22 (1) (2007) 69–80.
[72] P. Ruoff, L. Rensing, The temperature-compensated Goodwin model simulates many circadian clock properties, J. Theor. Biol. 179 (1996) 275–285.
[73] D. Gonze, S. Bernard, C. Waltermann, A. Kramer, H. Herzel, Spontaneous synchronization of coupled circadian oscillators, Biophysical Journal 89 (2005) 120–129.
[74] D. Gonze, Modeling circadian clocks: From equations to oscillations, Cent. Eur. J. Biol. 6 (5) (2011) 699–711.
[75] C. Vasalou, M. A. Henson, A multicellular model for differential regulation of circadian signals in the shell and core regions of the SCN, Journal of Theoretical Biology 288 (2011) 44–56.
[76] J. Xu, C. Gu, A. Pumir, N. Garnier, Z. Liu, Entrainment of the suprachiasmatic nucleus network by a light-dark cycle, Phys. Review E 86 (2012) 041903.
[77] C. Gu, J. Xu, Z. Liu, J. Rohling, Entrainment range of nonidentical circadian oscillators by a light-dark cycle, Phys. Review E 88 (2013) 022702.
[78] L. Pecora, T. Carroll, Master stability functions for synchronized coupled systems, Phys. Rev. Letters 80 (10) (1998) 2109–2112.
[79] A. Pogromsky, H. Nijmeijer, Cooperative oscillatory behavior of mutually coupled dynamical systems, IEEE Trans. Circuits Syst. - I 48 (2) (2001) 152–162.
[80] A. Pavlov, A. Pogromsky, N. van de Wouw, H. Nijmeijer, Convergent dynamics, a tribute to Boris Pavlovich Demidovich, Systems Control Lett. 52 (3-4) (2004) 257–61.
[81] G.-B. Stan, R. Sepulchre, Analysis of interconnected oscillators by dissipativity theory, IEEE Trans. Autom. Control 52 (2) (2007) 256–270.
[82] A. Hamadeh, G.-B. Stan, R. Sepulchre, J. Goncalves, Global state synchronization in networks of cyclic feedback systems, IEEE Transactions on Automatic Control 57 (2012) 478–483.
[83] A. Proskurnikov, M. Cao, Synchronization of Goodwin's oscillators under boundedness and nonnegativeness constraints for solutions, IEEE Trans. Autom. Control 62 (1) (2017) 372–378.
[84] A. Proskurnikov, F. Zhang, M. Cao, J. Scherpen, A general criterion for synchronization of incrementally dissipative nonlinearly coupled agents, in: Proceedings of European Control Conference (ECC 2015), Linz, Austria, 2015, pp. 581–586.
[85] C. Li, L. Chen, K. Aihara, Synchronization of coupled nonidentical genetic oscillators, Phys Biol 3.
[86] C. Li, L. Chen, K. Aihara, Stochastic synchronization of genetic oscillator networks, BMC Systems Biology 1 (1) (2007) 6.
[87] D.-H. Nguyen, S. Hara, Entrainment analysis in Goodwin–type nonlinear oscillator networks driven by external periodic signals, SICE Journal of Control, Measurement, and System Integration 7 (6) (2014) 337–346.
[88] D. Nguyen, S. Hara, Synchronization behaviors in goodwin oscillator networks driven by external periodic signals, in: Proc. of European Control Conference ECC-2013, 2013, pp. 4275–4280.
[89] Y. Wang, Y. Hori, S. Hara, F. Doyle, Intercellular delay regulates the collective period of repressively coupled gene regulatory oscillator networks, IEEE Trans. Autom. Control 59 (1) (2014) 211–216.
[90] D. Efimov, Phase resetting control based on direct phase response curve, J. Math. Biol. 63 (2011) 855–879.
[91] P. Sacre, R. Sepulchre, Sensitivity analysis of oscillator models in the space of phase-response curves: Oscillators as open systems, IEEE Control Syst. Mag. 34 (2) (2014) 50–74.
[92] H. Ahmed, R. Ushirobira, D. Efimov, On robustness of phase resetting to cell division under entrainment, J. Theor. Biol. 387 (2015) 206–213.
[93] D. Efimov, Phase resetting for a network of oscillators via phase response curve approach, Biol. Cybern. 109 (1) (2015) 95–108.
[94] A. Winfree, The Geometry of Biological Time, Springer, 1980.
[95] C. Johnson, Forty years of PRCs. What have we learned?, Chronobiology International 16 (6) (1999) 711–743.
[96] R. Goebel, R. Sanfelice, A. Teel, Hybrid dynamical systems, IEEE Contr. Syst. Mag. 29 (2) (2009) 28–93.
[97] R. Mirollo, S. Strogatz, Synchronization of pulse-coupled biological oscillators, SIAM J. on Appl. Math. 50 (6) (1990) 1645–1662.
[98] L. Abbott, C. van Vreeswijk, Asynchronous states in networks of pulse-coupled oscillators, Phys. Review E 48 (2) (1993) 1483–1490.
[99] P. Goel, B. Ermentrout, Synchrony, stability, and firing patterns in pulse-coupled oscillators, Physica D 163 (2002) 191–216.
[100] E. Brown, J. Moehlis, P. Holmes, On the phase reduction and response dynamics of neural oscillator populations, Neural Computation 16 (2004) 673–715.
[101] C. Canavier, S. Achuthan, Pulse coupled oscillators and the phase resetting curve, Mathematical Biosciences 226 (2010) 77–96.
[102] Y. Wang, F. Doyle, Optimal phase response functions for fast pulse-coupled synchronization in wireless sensor networks, IEEE Trans. on Signal Proc. 60 (10) (2012) 5583–5588.
[103] A. Mauroy, R. Sepulchre, Global analysis of a continuum model for monotone pulse-coupled oscillators, IEEE Trans. Autom. Control 58 (5) (2013) 1154–1166.
[104] F. Núñez, Y. Wang, F. Doyle, Global synchronization of pulse-coupled oscillators interacting on cycle graphs, Automatica 52 (2) (2015) 202–209.
[105] F. Núñez, Y. Wang, F. Doyle, Synchronization of pulse-coupled oscillators on (strongly) connected graphs, IEEE Trans. Autom. Control 60 (6) (2015) 1710–1715.
[106] F. Núñez, Y. Wang, A. R. Teel, F. J. Doyle, Synchronization of pulse-coupled oscillators to a global pacemaker, Systems & Control Letters 88 (2016) 75 – 80.
[107] F. Ferrante, Y. Wang, Robust almost global splay state stabilization of pulse coupled oscillators, IEEE Transactions on Automatic Control 62 (6) (2017) 3083–3090.
[108] A. Proskurnikov, M. Cao, Synchronization of pulse-coupled oscillators and clocks under minimal connectivity assumptions, IEEE Trans. Autom. Control 62 (11) (2017) 5873 – 5879.
[109] E. Izhikevich, Weakly pulse-coupled oscillators, FM interactions, synchronization, and oscillatory associative memory, IEEE Trans. on Neural Networks 10 (3) (1999) 508–526.
[110] Y. Kuramoto, Chemical Oscillations, Waves, and Turbulence, Springer, Berlin, 1984.
[111] Y. Kuramoto, Collective synchronization of pulse-coupled oscillators and excitable units, Physica D 50 (1991) 15–30.
[112] A. Papachristodoulou, A. Jadbabaie, U.Münz, Effects of delay in multi-agent consensus and oscillator synchronization, IEEE Trans. Autom. Control 55 (6) (2010) 1471 – 1477.
[113] A. Matveev, I. Novinitsyn, A. Proskurnikov, Stability of continuous-time consensus algorithms for switching networks with bidirectional interaction, in: Proc. Europ. Control Conference (ECC), 2013, pp. 1872–1877.
[114] S. H. Strogatz, From Kuramoto to Crawford: exploring the onset of synchronization in populations of coupled oscillators, Physica D: Nonlinear Phenomena 143 (1) (2000) 1 – 20.
[115] J. A. Acebrón, L. L. Bonilla, C. J. Pérez Vicente, F. Ritort, R. Spigler, The Kuramoto model: A simple paradigm for synchronization phenomena, Rev. Mod. Phys. 77 (2005) 137–185.
[116] F. Dörfler, F. Bullo, Synchronization in complex networks of phase oscillators: A survey, Automatica 50 (6) (2014) 1539–1564.
[117] F. A. Rodrigues, T. K. Peron, P. Ji, J. Kurths, The Kuramoto model in complex networks, Physics Reports 610 (2016) 1 – 98.
[118] C. Thron, The secant condition for instability in biochemical feedback control. I. the role of cooperativity and saturability, Bull. Math. Biol. 53 (3) (1991) 383–401.
[119] M. Arcak, E. Sontag, Diagonal stability of a class of cyclic sys-

tems and its connection with the secant criterion, Automatica 42 (2006) 1531–1537.
[120] H. Taghvafard, A. Proskurnikov, M. Cao, Local and global analysis of endocrine regulation as a non-cyclic feedback system, Automatica 91 (2018) 190–196.
[121] H. Taghvafard, A. Proskurnikov, M. Cao, Stability properties of the Goodwin-Smith oscillator model with additional feedback, IFAC-PapersOnLine 49 (14) (2016) 131–136.
[122] G. Enciso, H. Smith, E. Sontag, Nonmonotone systems decomposable into monotone systems with negative feedback, J. Differential Equations 224 (2006) 205 – 27.
[123] Y. Hori, M. Takada, S. Hara, Biochemical oscillations in delayed negative cyclic feedback: Existence and profiles, Automatica 49 (9) (2013) 2581–2590.
[124] X. Sun, R. Yuan, J. Cao, Bifurcations for Goodwin model with three delays, Nonlin. Dynamics 84 (2016) 1093–1105.
[125] J. Mallet-Paret, H. Smith, The Poincaré-Bendixson theorem for monotone cyclic feedback systems, J. Dynam. Diff. Equations 2 (4) (1990) 367–421.
[126] Y. Hori, T.-H. Kim, S. Hara, Existence criteria of periodic oscillations in cyclic gene regulatory networks, Automatica 47 (2011) 1203–1209.
[127] R. Potrie, P. Monzón, Local implications of almost global stability, Dynam. Syst. 24 (1) (2009) 109–115.
[128] J. Tyson, On the existence of oscillatory solutions in negative feedback cellular control processes, J. Math. Biol. 1.
[129] S. Hastings, J. Tyson, D. Webster, Existence of periodic solutions for negative feedback cellular control systems, J. Differential Equations 25 (1977) 39–64.
[130] A. Proskurnikov, M. Cao, H.-T. Zhang, Entrainment of Goodwin's oscillators by periodic exogenous signals, in: Proc. of 54th IEEE Conf. on Decision and Control, 2015, pp. 615–619.
[131] G. Katriel, Uniqueness of periodic solutions for asymptotically linear Duffing equations with strong forcing, Topological Methods in Nonlinear Analysis 12 (1998) 263–274.
[132] H. El Samad, D. Del Vecchio, M. Khammash, Repressilators and promotilators: Loop dynamics in synthetic gene networks, in: Proc. of American Control Conference (ACC-2005), 2005, pp. 4405–4410.
[133] R. Rao, D. DuBois, R. Almon, W. Jusko, I. P. Androulakis, Mathematical modeling of the circadian dynamics of the neuroendocrine-immune network in experimentally induced arthritis, American Journal of Physiology - Endocrinology and Metabolism 311 (2) (2016) E310–E324.
[134] M. Krupa, A. Vidal, F. Clément, A network model of the periodic synchronization process in the dynamics of calcium concentration in gnrh neurons, Journal of Mathematical Neuroscience 3 (4).
[135] F. C. W. Wu, D. C. Irby, I. J. Clarce, J. T. Cummins, D. M. de Kretse, Effects of gonadotropin-releasing hormone pulse-frequency modulation on luteinizing hormone, foilicle-stimulating hormone and testosterone in hypothalamo/pituitary-disconnected rams, Biology of Reproduction 37 (10) (1987) 501–505.
[136] A. Medvedev, A. Churilov, A. Shepeljavyi, Mathematical models of testosterone regulation, Stochastic optimization in informatics 2 (2006) 147–158.
[137] A. Gelig, A. Churilov, Stability and oscillations of nonlinear pulse-modulated systems, Birkhäuser, Boston, 1998.
[138] Z. Zhusubaliyev, A. Churilov, A. Medvedev, Bifurcation phenomena in an impulsive model of non-basal testosterone regulation, Chaos: An Interdisciplinary Journal of Nonlinear Science 22 (2012) 013121–1–013121–11.
[139] P. Mattsson, A. Medvedev, Z. Zhusubaliyev, Pulse-modulated model of testosterone regulation subject to exogenous signals, in: Proceedings of the 55th IEEE Conference on Decision and Control, Las Vegas, NE, 2016, pp. 5023–5028.
[140] V. S. Afraimovich, L. P. Shilnikov, Invariant two-dimensional tori, their breakdown and stochasticity, Amer. Math. Soc. Transl. 149 (1991) 201–211.
[141] D. G. Aronson, M. A. Chory, G. R. Hall, R. P. McGehee, Bifurcations from an invariant circle for two parameter families of maps of the plane: A computer-assisted study, Commun. Math. Phys. 83 (1982) 303–353.
[142] V. Maistrenko, Y. Maistrenko, E. Mosekilde, Torus breakdown in noninvertible maps, Physical Review E 67 (2003) 046215–1 – 046215–6.